Improving the Performance of Silica Nanoparticles in Cementitious Media

By

Abbas Ahmed Albu Shaqraa

A dissertation submitted in partial fulfillment of

the requirements for the degree of

Doctor of Philosophy

(Civil Engineering)

at the

UNIVERSITY OF WISCONSIN – MADISON

2022

Date of final oral examination: 11/07/2022

The dissertation is approved by the following members of the Final Oral Committee:

Bu Wang, Assistant Professor, Civil and Environmental Engineering (Advisor)

Pavana Prabhakar, Associate Professor, Civil and Environmental Engineering

Hannah Blum, Assistant Professor, Civil and Environmental Engineering

Ramathasan Thevamaran, Assistant Professor, Engineering Physics

This work is dedicated to my father,

Ahmed Albu Shaqraa,

for being my first teacher,

and my mother,

Lameah Al Sulaiman,

for being my role model,

and my wife,

Sakenah Alsalem,

and my children,

Ahmed and Kawthar,

with all the love.

Abstract

In aqueous solutions, silica nanoparticles coagulate upon the adsorption of calcium ions which reduces the reactivity of these particles in lime-based materials. This issue limits the application of silica nanoparticles in cementitious materials, even though they are excellent pozzolans that have the potential to significantly enhance the performance and durability of concrete. To mitigate this issue, we propose to temporarily remove calcium ions from the cementitious solution at the very early stage of the reaction (e.g. during mixing) to reduce the possibility of nanoparticles agglomeration.

The current study evaluates the proposed approach by investigating the effect of calcium chelators on the reactivity of silica nanoparticles in $Ca(OH)_2$-SiO_2 system. Dynamic light scattering measurements, isothermal calorimetry, thermogravimetry, and compressive strength tests were performed to assess the performance of chelators in the calcium hydroxide-silica nanoparticles system. Results indicate that calcium chelators could effectively improve the reactivity of silica nanoparticles as reflected in their higher ultimate heat of reaction by isothermal calorimetry test. Calcium chelator with EDTA caused the highest ultimate heat of reaction implying its superior performance compared to other chelators. TGA results confirmed the data obtained from the calorimetry test. In addition, utilization of EDTA resulted in the highest compressive strength among the samples with and without calcium chelators. The exponential technique was used to determine apparent activation energy values, and the model perfectly fits the experimental calorimetric data.

The findings of this study suggest a possible solution to the problem of agglomeration of silica nanoparticles in lime-based materials. Besides, this study can be used to predict the apparent

activation energy of lime systems containing silica nanoparticles with and without pH elevation. Even though this study is on lime-based materials, the outcomes can be used to apply silica nanoparticles in developing high-performance cementitious materials in pavement-structure layers, cement and lime-stabilized soils, and building construction.

Acknowledgments

First, I am grateful to my thesis advisor Prof. Bu Wang for his appreciated advice, encouragement, and support throughout this course of research. Prof. Wang helped me to resolve the challenges I faced while conducting my research. He provided a friendly environment and appealing insights.

After that, I would like to express my most profound sense of gratitude to the research scientist Dr. Payam Hosseini. Thank you for contributing your time, energy, and knowledge to help me accomplish my goals. I look forward to future collaborations, as our research interests will certainly invite further cooperation.

Moreover, I am thankful to my committee members, Profs. Pavana Prabhakar, Hannah Blum, and Ramathasan Thevamaran for their constructive comments on my dissertation, assistance, and understanding.

Finally, I acknowledge the civil and environmental engineering department at the University of Wisconsin – Madison for providing appreciated guidance throughout my graduate program and offering this valuable opportunity to pursue my studies and develop my research abilities. Thank you!

Table of Contents

List of Tables

List of Figures

Chapter 1

Introduction

1.1 Cement hydration

Portland cement is composed mainly of the following four chemical phases: tricalcium silicate (C_3S), dicalcium silicate (C_2S), tricalcium aluminate (C_3A), and tetra calcium aluminoferrite (C_4AF). The typical portland cement clinker contains 50 to 70% of C_3S, 15 to 30% of C_2S, 5 to 10% of C_3A, and 5 to 15% of C_4AF (Kosmatka et al. 2011).

Portland cement is a hydraulic cement that is set and hardened by reacting chemically with water to form new compounds that are the main components of the hardened cement paste. After the initial high rate of hydration, mainly because of C_3A, the hydration rate gets very low. This period of slow thermal activity is known as the dormant period and is sometimes called an induction period. The dormant (induction) period lasts for several hours, during which the cement paste is workable and can be handled. Most of the hydration and strength development occurs within the first month of mixing, and they continue slowly for a long time (Kosmatka et al. 2011).

C_3S and C_2S hydrate and form calcium hydroxide (CH) and calcium silicate hydrate (C-S-H). C_3S hydrates and hardens rapidly and is mainly responsible for initial and early strength. C_2S hydrates and hardens slowly and contributes largely to strength increase at ages beyond one week. C_3A contributes slightly to early strength development. C_4AF does not play a significant role in strength but gives cement its characteristic gray color. Hydrated cement paste contains 15% to 25% CH and about 50% C-S-H by weight. The strength of the hydrated cement is primarily owing

to C-S-H. The early strength of cement is higher with increased percentages of C_3S (Kosmatka et al. 2011).

The major cementitious binder in hardened portland cement is C-S-H, which is commonly referred to as the glue that binds the whole components in the matrix. CH does not contribute to the strength and has a marginal effect on the mechanical properties of the hydrated cement paste. Because CH is easily leached out by dissolution and diffusion and can be attacked by chemicals like acids and sulfates. It is frequently found as a weak link since it does not show any binding effect in cement-based materials. But it maintains the high pH needed to stabilize the C-S-H (Kosmatka et al. 2011, and Aïtcin et al. 2016).

1.2 Pozzolanic reactivity

The pore fluid provides the environment for cement hydration in which calcium, silicon, and hydroxyl released by the cement clicker convert to C-S-H and CH. The calcium and pH influence the dissolution of cement clinker and the perception of hydration products (Chen et al. 2018).

Kosmatka et al. 2011 discussed that the siliceous pozzolans can react with the CH produced by the hydration of portland cement, resulting in the formation of additional C-S-H leading to more strength and less permeability on the hardened material. Yajun et al. 2004 further described the pozzolanic reactivity as the chemical reaction between silica particles and calcium hydroxide in the presence of moisture to form C-S-H, according to the following equation:

$$1.1\ Ca(OH)_2 + SiO_2 + 2.8\ H_2O \rightarrow C_{1.1}\text{-}S\text{-}H_{3.9} \qquad \text{(Eq.1.1)}$$

The pozzolanic materials have long been utilized in cement-based materials to partially replace portland cement. However, the C-S-H formed by the pozzolanic reaction may slightly have a different composition and structure than those produced by the hydration of portland cement (Kosmatka et al. 2011).

Silica fume, referred to as micro-silica, is a byproduct of the silicon and ferrosilicon industries, is commonly used to improve the durability and mechanical performance of cement-based materials. The fundamental advantage of silica fume is its faster pozzolanic reaction compared to other pozzolans because of its high purity of silica and high specific surface area (Madani et al. 2012). Silica fume is typically used in amounts between 5% and 10% by the mass of the total cementing material. It is used in applications where a high degree of impermeability is needed and high-strength concrete (Kosmatka et al. 2011).

Various nanosized amorphous silica has become available. Because these materials have a higher specific surface area than silica fume, there has been a lot of interest in studying the effects of silica nanoparticles on the characteristics of cement-based materials (Madani et al. 2012). Silica nanoparticles also have a very high pozzolanic reactivity and may fill the pores in the cementing matrix (Zhuang et al. 2019).

1.3 Performance of silica nanoparticles in cement-based materials

Silica nanoparticles have a four-fold performance in cementitious media (Hosseini et al. 2010). Silica nanoparticles were believed to act as nucleation sites of cement hydration, participate in the pozzolanic reaction to form C-S-H, accelerate the cement hydration, fill the voids in the cement matrix, and prevent the growth of ettringite and CH crystals.

Zhuang et al. 2019 reported that silica nanoparticles influenced the macro characteristics and microstructure of the cementing system. The mass of hydrated calcium silicate gels and ettringite crystal gradually increased with the increase of silica nanoparticles concentration within a specified dose range. The addition of silica nanoparticles to the cementing system can accelerate the early hydration, which helps develop early strength.

Although the addition of silica nanoparticles may not significantly improve the mechanical performance, it can substantially reduce chloride ion penetration and help to prevent steel bar corrosion in reinforced concrete. Also, it improves the interfacial strength, refines the pores, and reduces the water permeability (Zhuang et al. 2019). However, higher silica nanoparticles concentrations showed a negative effect and damaged the microstructure of the cement matrix due to their accumulation (Metaxa et al. 2021).

For more than two decades, colloidal silica nanoparticles dispersed in a liquid medium were available to the construction industry, and they were incorporated into several field projects (Belkowitz et al. 2014).

Examples include the taxiway pavements of the Eagle County Airport complex. The concrete pavement mixtures contained portland cement, class F fly ash, colloidal silica, coarse aggregates, sand, high-range water-reducing admixture, and air-entraining admixture (Belkowitz et al. 2014). For the paving application, 8 m^3 of concrete was poured. The workability of the mixtures was unaffected by the colloidal silica incorporation and additional on-site water-reducing admixtures were not needed. Colloidal silica increased the strength development and durability of concrete, according to tests performed in the field and laboratory. Compared to the control mixtures, the mixtures made with colloidal silica showed higher compressive strength at all testing ages (1, 4, 7, and 28 days) reaching 62 MPa at 28 days. Also, colloidal silica reduced the rate of

alkali-silica reaction (ASR) of aggregate and showed a low risk of deleterious expansion in mortar mixtures.

Another example is the U.S. Army Corps of Engineers project, where colloidal silica was used in grout to match the physical characteristics of the existing rock. The grout mixture included cement, fine hematite aggregates, fine silica aggregates, silica fume, colloidal silica, and chemical admixtures. The colloidal silica was used as a viscosity modifier to prevent segregation and replace sodium bentonite clay, typically used in this application. The unconfined compressive strength of the grout was 91 MPa (ACI Committees 236 and 241 in 2017).

In addition, it was used as a viscosity-modifying agent in self-consolidating concrete in a project near Venice, Italy. The slump flow was 700 to 800 mm. The concrete mixture included portland cement, blast furnace slag, fly ash, colloidal silica, and polyacrylate high-range water-reducing admixture with retarding effect. The 28th-day compressive strength was 40 MPa (ACI Committees 236 and 241 in 2017).

1.4 Dispersion of silica nanoparticles in cementitious media

According to Madani et al. 2012, the silica nanoparticles use was different from silica fume, wherein no reduction in calcium ion concentration was observed during the hydration of cement in the case of incorporating silica fume. Silica nanoparticles consumed calcium ions in the first hours of hydration of cement through the following reaction where each calcium ion can create a bridge between two silica particles:

$$SiO^{-} + Ca^{2+} + {}^{-}OSi \rightarrow SiO^{-+}Ca^{+-}OSi \qquad \text{(Eq.1.2)}$$

Madani et al. 2012 had further discussed that the adsorption of silica nanoparticles to calcium ions on the surface of silica particles lowers the electrostatic forces between particles, contributing to their aggregations. During the first hours of cement hydration, the surface of silica aggregates is clean. By the progress of hydration, a layer of silicate hydrate thickens with time forms on the surface of silica aggregates, and this layer slows down the dissolution of silica particles. Hence, the rate of pozzolanic reactivity is controlled by the dissolution rate of silica in the pore fluid. This point of view, which may need further consideration, is that the fast pozzolanic reaction during early ages of hydration of cement might be due to the release of the large siliceous ions of silica nanoparticles, which reduce over time due to the formation and precipitation of silicate hydrate on the surface of silica aggregates.

The same observation was discussed by Reches et al. 2018. They found that adding CH to silica nanoparticles caused the silica nanoparticles suspension to adsorb calcium ions (Zeta potential was -30 mV and became +15mV in DI water). As the concentration of CH increased, the thickness of the diffuse electrical layer decreased (and Zeta potential reached zero). Then, the silica nanoparticles agglomerated through a reduction in the electrostatic repulsive forces between silica nanoparticles, and then the calcium ions bridge the surfaces of silica nanoparticles.

1.5 Application of calcium chelating agents in cement-based materials

Calcium chelating agents have long been used in cement-based materials as a retarder of cement hydration since they can remove calcium ions from the cement pore fluid. They cause an initial flush of silicon ions into the cement pore fluid during the very early hydration age. When the silica is substantially precipitated as C-S-H, only when the chelating agent is saturated, more calcium become available by hydration, and more intensified precipitation of C-S-H gel is expected (Thomas et al. 1983).

1.6 Problem statement and research objectives

Silica nanoparticles have shown a superior effect in cementitious materials because of their fine particle size and high pozzolanic reactivity. They significantly contributed to early age strength and durability performance. However, previous studies showed that silica nanoparticles immediately agglomerate when added to calcium-rich media such as portland cement or lime. This phenomenon is simply described by the bridging effect of calcium ions to silica, where each calcium ion creates a bridge between two silica particles leading to their agglomeration. Different mixing procedures and dispersion methods were applied to resolve the problem of silica nanoparticles agglomeration in cementitious media. These methods mainly include pre-mixing silica nanoparticles in water with or without surfactants, high shear mixing, and direct or indirect sonication. Although some of these techniques improved the dispersion of silica nanoparticles in cementitious materials, they are not economical and may not be applicable at the industry level.

This study considers using calcium chelating agents. They have long been used in cement-based materials as retarders of cement hydration. Since they can remove calcium ions from the cementitious matrix, they cause an initial flush of silicon ions at a very early age. When the calcium chelating agent is saturated, more calcium becomes available for reaction. Hence, the rate of pozzolanic reactivity is controlled by the dissolution rate of silica in the pore fluid. The findings of this study can be used to produce modified lime systems containing better-dispersed silica nanoparticles for enhanced pozzolanic reactivity.

Since better dispersion of silica nanoparticles in cementitious media would result in better performance in terms of higher compressive strength and finer pore structure, the objective of this study is to investigate the use of different calcium chelating agents to enhance the dispersion of silica nanoparticles during the mixing period by preventing their agglomeration leading to

enhancement of compressive strength and pore structure. In addition, the activation energy was calculated to explore the temperature sensitivity of mixture responses using complex modeling.

1.7 Dissertation structure and research plan

This dissertation is divided into three chapters. The first chapter includes the introduction, objectives, and phases of the research. The research is conducted in three phases. The phases of this research are as follows:

Phase I: Thermodynamic modeling is used in the first phase of this study to examine the impact of silica nanoparticles concentration on the pozzolanic reaction in lime pastes. The ratio of calcium hydroxide to silica nanoparticles (C/S) would be chosen based on the minimum and maximum ratios necessary to accomplish the complete reaction of all silica nanoparticles.

Phase II: This phase investigates the effect of three different calcium complexing agents, including the EDTA disodium salt dihydrate, oxalic acid, and potassium oxalate monohydrate, on the pozzolanic reactivity of silica nanoparticles in lime pastes.

First, the particle size distribution of silica nanoparticles would be measured in different aqueous solutions, including deionized water, saturated calcium hydroxide, and a saturated calcium hydroxide solution containing EDTA.

Next, the effect of the calcium chelating agents on the heat flow and cumulative heat released by silica nanoparticles-lime pastes will be measured by isothermal calorimetry and modeled.

After that, using thermogravimetric analysis (TGA), the amount of $Ca(OH)_2$ consumed during pozzolanic reaction would be measured to validate further the effect of calcium chelating agents on the extent of pozzolanic reactivity of silica nanoparticles.

Finally, the effect of the calcium chelating agents on the compressive strength of silica nanoparticles-lime mortars will be investigated. The mechanical compressive strength will be measured and compared to the control mixture (without a calcium chelating agent). This way, one can explore the role of calcium complexing agents in improving the pozzolanic reactivity of silica nanoparticles.

Phase III: In this phase, two types of silica nanoparticles with different specific surface areas and particle sizes were used to make lime pastes. They were tested at various temperatures, including 30, 40, and 50 °C, with and without pH elevation. The isothermal calorimetric data were studied to calculate the heat flow and cumulative heat output. The reaction heat rates were later computed using an exponential technique. Furthermore, the impact of using EDTA was analyzed and compared to tests conducted without it. Finally, the apparent activation energy was calculated using the Arrhenius equation, and exponential technique.

Phases I and II are covered in Chapter 2. Chapter 3 discusses phase III. The summary and conclusion of the study are presented at the end of this dissertation.

Chapter 2

The reactivity of silica nanoparticles with calcium hydroxide

2.1 Introduction

Lime is an ancient binding material that has been utilized for centuries (Stefanidou et al. 2005, and Zhang et al. 2011). Various reasons make lime still appealing, including the availability of its raw materials, low cost of manufacture, and ease of usage. The principal sources of lime are natural rocks rich in calcium carbonates ($CaCO_3$), such as limestone, dolomite, and chalk. In actual production, $CaCO_3$ is calcined at 1000-1100 °C to form calcium oxide (CaO), often known as quicklime. Industrial wastes are another source of lime. For example, the carbide slag produced during the acetylene manufacturing process is predominantly constituted of calcium hydroxide ($Ca(OH)_2$), often known as hydrated lime (Zhang et al. 2011). Because of its adhesive and binding properties, lime is diluted in water and combined with sand to form a lime mortar. Such mortar has been widely studied for use in the production of construction joints, non-load-bearing partitions, ceilings, and the painting of interior and exterior walls of buildings (Stefanidou et al. 2005, and Zhang et al. 2011). Lime is also regarded as a base stabilizer to control volume change and increase soil strength, as described by various researchers (Stefanidou et al. 2005, Zhang et al. 2011, Basma et al. 1991, Phanikumar 2009, and Pu et al. 2019).

Basma et al. 1991, and Phanikumar 2009 discussed that lime reduces the volume change potential through the cation exchange of calcium ions with monovalent soil cations, resulting in increased calcium ions concentration in the pore solution. The increased concentration of calcium ions causes flocculation and agglomeration of soil particles. This short-term soil modification

phenomenon changes the soil texture by increasing the proportion of coarse particles. However, the long-term phenomena, including the lime carbonation and pozzolanic reactions, strengthen the soil over time. From the results obtained by Phanikumar 2009, the plasticity index of an expansive soil dropped instantaneously to about one-third after lime treatment, resulting in an immediate strength enhancement. The plasticity index was 73, then dropped to 25 at a lime content of 6% by the dry weight of the soil. Also, Pu et al. 2019 detected increased compressive strength of silt when lime was used with or without cement. However, a pronounced effect was observed when lime was combined with cement. According to their findings, the 7-day compressive strength reached 79 kPa when lime was used without cement and 178 kPa when lime was mixed with cement. Recently, studies have been conducted using nanomaterials to improve the performance of lime and cement materials (Joju et al. 2021, and Nunes et al. 2016). However, most of the research incorporating nanomaterials has focused on improving the performance of cement. In contrast, lime has received less attention (Nunes et al. 2016).

Literature indicates that silica nanoparticles considerably improve the properties of cementitious and lime materials (Joju et al. 2021, and Kannan et al. 2021). Silica nanoparticles were believed to participate in the pozzolanic reaction to form calcium silicate hydrates (C-S-H) and fill the voids in the lime matrix resulting in improved compressive strength and reduced pore volume in the structure (Alvarez et al. 2013). The increase in the 7-day compressive strength was reported in the studies to be equal to four times, reaching 12.7 MPa in lime mortar when silica nanoparticles were incorporated (Fernández et al. 2013). These authors also detected the filling effect of silica nanoparticles in lime mortar by measuring the pore size distribution. The mean pore diameter was reduced from 0.8 to 0.2 μm when silica nanoparticles were employed, demonstrating the densification effect on the matrix. Also, Kannan et al. 2021 discovered that combining silica

nanoparticles with lime improved a high plastic clay soil strength by approximately five times. But, when silica nanoparticles were used without lime, they only enhanced the soil strength by about two times.

According to Hosseini et al. 2018, previous studies used various types of silica nanoparticles in cementitious systems. The main types include pyrogenic, precipitated, and hydrosols. Pyrogenic and precipitated silica nanoparticles are generally in agglomerates that are difficult to disperse in water. In contrast, hydrosols silica nanoparticles are monodispersed particles in water. Further, it was discovered that finer nanoparticles had stronger pozzolanic activity than coarser ones because the rate of the pozzolanic reactivity is accelerated by more silica dissolution in the pore fluid (Khaloo et al. 2016 and, Madani et al. 2012). However, finer silica nanoparticles produced more agglomerates than the coarser ones. Overall, photographs taken with an optical microscope of a lime suspension containing silica nanoparticles revealed a denser matrix due to silica incorporation. Still, large agglomerates of silica particles formed and did not contribute to the pozzolanic reaction (Fernández et al. 2013).

This research aims at exploring the dispersion behavior of silica nanoparticles in lime media. First, the effect of silica nanoparticles concentration on the pozzolanic reaction in lime pastes was investigated using thermodynamic modeling. Next, the agglomeration state and particle size distribution in various aqueous media containing silica nanoparticles were examined to demonstrate the influence of the EDTA chelating agent on improving the dispersion of silica nanoparticles in lime media. Then, the effect of three different calcium chelating agents, including the Ethylenediaminetetraacetic (EDTA) disodium dihydrate, potassium oxalate monohydrate, and oxalic acid dihydrate, on the pozzolanic reactivity of silica nanoparticles was investigated. The heat flow, cumulative heat released were measured and compared to the control mixture (without

a calcium chelating agent). After that, using thermogravimetric analysis (TGA), the amount of calcium hydroxide consumed during the pozzolanic reaction was measured to validate the calcium chelating agents further. Finally, the mechanical compressive strength was measured and compared to the control mixture (without a calcium chelating agent).

2.2 Materials and methods

2.2.1 Materials

Analytical reagent grade calcium hydroxide (≥95%, Fisher Scientific) and colloidal silica nanoparticles monodispersed in water (50% solid content, Nouryon) were used as the binding materials in lime pastes. The average particle size of calcium hydroxide powder and silica nanoparticles were 13 μm and 66 nm, respectively (Fig. A.1, Appendix A). Deionized (DI) water was used to prepare lime paste mixtures. In addition, to investigate the effect of calcium chelating agents, three types of chelators were employed. Analytical reagent grade ethylenediaminetetraacetic acid (EDTA) disodium salt dihydrate (≥99%, Thermo Scientific) as a calcium complexing chelator, and oxalic acid dihydrate (≥99%, Sigma Aldrich) and potassium oxalate monohydrate (98.5-101.0%, Thermo Scientific) as calcium binding chelator through chemical reactions were utilized in this study. Both oxalic acid and potassium oxalate react with calcium ions to produce an insoluble product, calcium oxalate. However, the former reduces the pH of the mixing water as a weak acid while the latter increases the pH upon its dissolution in water. Note that for the calcium chelators employed in this study, EDTA and oxalate ion are the chelating ligands that bind with calcium ions. Graded standard silica sand conforming to ASTM C778 was used to prepare lime mortars.

2.2.2 Experimental program

To initially examine the effect of calcium chelator on the dispersion of silica nanoparticles, particle size measurement experiments were performed through dynamic light scattering (DLS) measurements using Zetasizer Nano ZSP (Malvern Panalytical). Silica nanoparticles (with or without 20mM chelator) were added into a cuvette filled with DI or saturated $Ca(OH)_2$ solution (liquid/SiO_2 weight ratio of 100) and mixed for one minute. The particle size distribution of nanoparticles (with or without chelator) in DI and $Ca(OH)_2$ solution was then measured and compared.

Lime pastes were made at a $Ca(OH)_2/SiO_2$ (C/S) weight (wt.) ratio of 5 to ensure the availability of calcium hydroxide for possible reaction of entire silica nanoparticles as well as the existence of an unlimited source of calcium ions (with respect to silica) for continuous agglomeration of nanoparticles in the pore fluid during curing process. C/S ratio was selected based on the thermodynamic modeling using GEM-Selektor v.3.9.5 (Kulik et al. 2013, and Wagner et al. 2012), and CEMDATA18 database (Lothenbach et al. 2019) which indicated that the minimum and maximum C/S ratio of 0.84 and 2.01, respectively, is required to achieve all SiO_2 particles fully reacted (Fig. 2.1).

Among calcium chelators utilized in this study, ethylenediaminetetraacetic acid (EDTA) disodium salt dihydrate has the lowest solubility in water about 300mM (Davies et al. 2006) and thus, all calcium chelators were employed at 250mM. Liquid (DI water including the water in colloidal silica) to solid (dry silica nanoparticles and calcium hydroxide powder) (L/S) was selected as 1.5 to provide high fluidity to achieve well dispersion of nanoparticles and for ease of sample preparation. Table 2.1 shows the mix designs of lime pastes with and without calcium chelators.

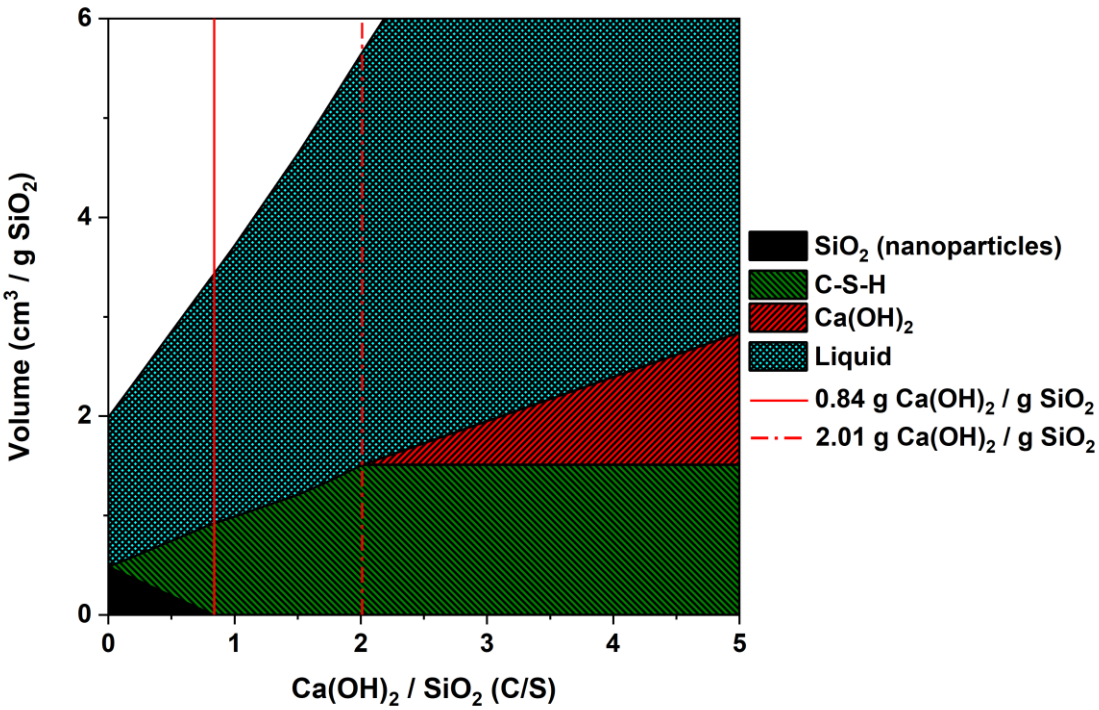

Figure 2.1 Influence of $Ca(OH)_2$ quantity on the consumption of 1 g SiO_2 in lime paste (L/S = 1.5).

Table 2.1 Lime paste mix designs.

Mix	C/S	L/S	Chelator (mM)
Control	5	1.5	NA
Chelator-incorporated	5	1.5	250

To prepare lime pastes, water (with or without dissolved chelator) and colloidal silica were added to calcium hydroxide in the mixing bowl and the whole mixture was mixed by a vacuum mixer for 4 minutes at a speed of 450 rpm. Vacuum mixer was used to minimize the carbonation of calcium hydroxide during sample preparation. After mixing, fresh lime paste was poured into the vials for calorimetry and thermogravimetric analysis (TGA). TAM Air isothermal calorimeter (TA Instruments) and Discovery TGA 550 (TA Instruments) were employed to assess the reactivity of silica nanoparticles in lime paste samples at various curing ages. For isothermal calorimetry, 7-10g of lime paste was transferred into a calorimetry vial, sealed, and lowered into the measuring position. Calorimetry was set at 25 ^{o}C and heat flow and cumulative heat were measured up to two weeks. Note that all calorimetry results in the $Ca(OH)_2$-SiO_2 systems with chelators were subtracted from the data collected from the corresponding $Ca(OH)_2$-chelator systems to account for any heat exchange caused by the interaction between the chelators and the source of calcium ions i.e., $Ca(OH)_2$. The outcome was then normalized to the weight of SiO_2 in the sample to facilitate comparison among various systems. The average heat flow and cumulative heat of reaction of two tested samples for each mixture were taken as the representative value.

For TGA, lime paste samples were cast in 20 mL vials and sealed cured at a temperature of 25±1 ^{o}C until the specified ages (7 and 28 days). At each specific age, approximately 20-30 mg sample was transferred into the TGA pan and the analysis was conducted by heating from 23 ^{o}C to 1000 ^{o}C, at a rate of 10 ^{o}C/min in N_2 atmosphere. The amount of consumed $Ca(OH)_2$ in the lime pastes was then calculated using tangential method to calculate the onset and end of its decomposition in the weight loss curve. The average of two tested samples for each mixture were taken as the representative value.

In addition to thermal analysis, the effect of calcium chelators on dispersion of silica nanoparticles within $Ca(OH)_2$-SiO_2 system was indirectly quantified through measuring compressive strength of lime mortar samples. Lime mortar mixtures with sand to binder (calcium hydroxide and silica nanoparticles) wt. ratio of 2.5, C/S wt. ratio of 1, and liquid (water) to binder (L/B) wt. ratio of 1.4 were made, sealed, and cured in an electric oven at 50 ^{o}C for 14 days. Due to very low strength of lime mortar samples, elevated temperature curing was conducted to accelerate the reaction between calcium hydroxide and SiO_2. To prepare lime mortars, lime pastes were made the same way mixtures for thermal experiments were produced using vacuum mixer. Thereafter, paste mixture was transferred into a bowl of rotary mortar mixer. Sand was added to the lime paste within 30 seconds at a mixing speed of 140 rpm. The whole mixture was mixed for 30 more seconds at the same speed. Subsequently, the mixer was stopped, and the mixture was allowed to rest for 30 seconds while the mixer wall was scraped, and the mixture was transmitted to the middle of the bowl. Finally, mortar mixture was mixed at a speed of 285 rpm for 90 seconds. The prepared mixture was then poured into 50-mm cubic molds sealed cured in the oven. At the age of 14 days, mortar samples were tested for compressive strength using SATEC^{TM} static hydraulic compression testing machine (Instron). The average compressive strength of three tested specimens for each mixture was taken as the representative value.

2.2.3 Reaction modeling

To obtain the ultimate cumulative heat of reaction in $Ca(OH)_2$-SiO_2 systems with and without calcium chelators, an exponential model (Eq. 2.1) which is the first-order model of reaction kinetics in heterogeneous solid state systems was adopted. This model has been proved to be applicable to lime-silica mixtures (Maddalena et al. 2019 and, Vyazovkin et al. 1997).

$$H(t) = b + H_o[1 - \exp(-kt)] \quad \text{(Eq. 2.1)}$$

where H(t) is the cumulative heat of reaction (J/g SiO_2) at time t(h), b is a constant factor to account for the initial spike in the heat flow (J/g SiO_2), H_o is the ultimate cumulative heat (J/g SiO_2), and k is a temperature-dependent rate constant of the reaction (h^{-1}).

2.3 Results and discussion

2.3.1 Particle size distribution

Fig. 2.2 shows the particle size distribution of silica nanoparticles dispersed in various media; deionized water (DI), saturated $Ca(OH)_2$ solution (CH), and saturated $Ca(OH)_2$ solution with EDTA as chelator (CH & EDTA). As can be seen in Fig. 2.2, once dispersed in saturated $Ca(OH)_2$ solution, silica nanoparticles agglomerate forming large aggregates tending to precipitate (i.e., separation of solid particles and dispersing medium or liquid as seen in the cuvette C containing calcium hydroxide and silica nanoparticles). The existence of calcium ions in the dispersing medium caused the average particles size of silica nanoparticles to increase from 66 nm (in DI) to 1731 nm (in CH) indicating that calcium ions have a strong binding effect. Nonetheless, upon incorporation of a calcium ion chelator (sodium salt of EDTA in this case) the average particle size of silica nanoparticles was reduced to 191 nm. This can be due to the complexation of calcium ions in the solution reducing the available ions to bind silica nanoparticles leading to large agglomerates.

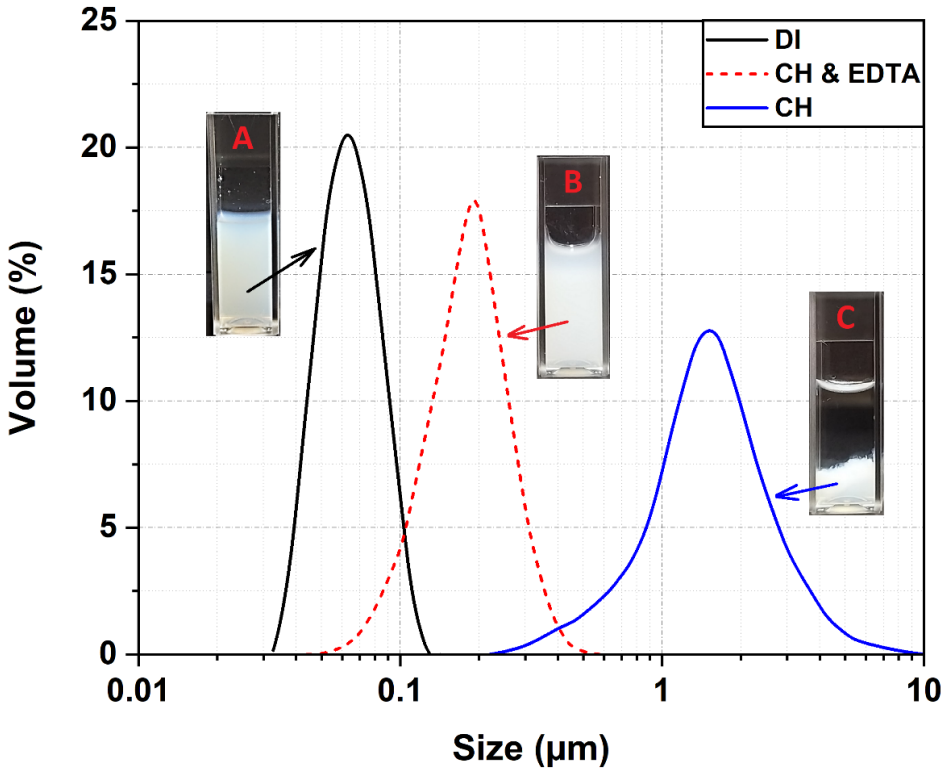

Figure 2.2 Particle size distribution of silica nanoparticles in various dispersing media: DI (deionized water), CH (saturated solution of calcium hydroxide), and CH & EDTA (saturated solution of calcium hydroxide incorporating 20mM EDTA as calcium chelator).

2.3.2 Thermal analysis

2.3.2.1 Isothermal calorimetry

Measuring the heat absorbed/liberated by a chemical reaction is a direct way to quantify the reaction kinetics. Reaction between $Ca(OH)_2$ and SiO_2 is an exothermic reaction releasing heat to the environment (Snellings et al. 2012). As such, higher heat of reaction can be translated into the production of more C-S-H. Since C/S weight ratio is 5, according to thermodynamic calculations (Fig. 2.1), SiO_2 quantity controls the total reaction as there is more calcium hydroxide than the required amount to fully react with SiO_2 in the system. This means that higher heat of reaction in the studied system corresponds to higher quantity of reacted SiO_2. In $Ca(OH)_2$-SiO_2 systems, due to their very high surface area, silica nanoparticles rapidly dissolve leading to faster production of C-S-H. Also, the unreacted nanoparticles provide sites for nucleation of C-S-H accelerating the reactivity in the system (Hosseini et al. 2010). However, if agglomerated, a large quantity of nanoparticles is entrapped in the aggregate causing less particles available to react within the system (Khaloo et al. 2016, and Madani et al. 2012). In other words, agglomeration of silica nanoparticles results in decreasing their reactivity leading to lower heat of reaction. Therefore, isothermal calorimetry can be used to indirectly quantify the agglomeration state of silica nanoparticles in $Ca(OH)_2$-SiO_2 systems.

As Fig. 2.3 shows, addition of various calcium chelators affects the reactivity of silica nanoparticles in the lime system. According to Fig. 2.3, for control system i.e., without the application of chelator, there is a spike in heat flow which can be due to the dissolution of $Ca(OH)_2$ and SiO_2 and very initial interaction of ions in the solution followed by a rather small and broad peak in the heat flow (main reaction peak). The region between these two peaks which corresponds to a constant heat flow is called induction period indicating very slow activity after which time an

acceleration of reaction happens (Lothenbach et al. 2019). As seen in Fig. 2.3, calcium chelators alter the main course of reaction in the lime-silica nanoparticles system. The addition of potassium oxalate (Eq. 2.2) increases the pH of the solution in the lime paste (Iler 1979, and Chen et al. 2018), resulting in more dissolution of amorphous silica nanoparticles. This leads to higher reactivity of silica nanoparticles as indicated by a high main peak in the heat flow curve. On the other hand, oxalic acid (Eq. 2.3) reduces the pH (Chen et al. 2018), causing less silica nanoparticles to dissolve inducing lower main reaction peak in the heat flow (Fig. 2.3).

$$K_2C_2O_4 + Ca(OH)_2 \rightarrow CaC_2O_4 + 2KOH \quad \text{(Eq. 2.2)}$$

$$H_2C_2O_4 + Ca(OH)_2 \rightarrow CaC_2O_4 + 2H_2O \quad \text{(Eq. 2.3)}$$

In the case of utilizing EDTA as calcium chelating agent, an extended induction period was observed, and the main peak's height is lower than that of control lime paste (without any chelator). EDTA complexes with calcium ions removing them from the solution while inducing no chemical reaction. This means that there is no heat exchange due to the complexation of calcium ions by EDTA molecules. Removal of calcium ions reduces their availability in the solution and thus, $Ca(OH)_2$-SiO_2 reaction is delayed. However, this is not the case for chelators with oxalate ligand (e.g., potassium oxalate and oxalic acid). For these chelators, calcium ions react with oxalate ions forming an insoluble compound in aqueous media, calcium oxalate, precipitating in the matrix. Undissolved silica nanoparticles can act like nucleation sites to precipitate calcium oxalate leading to its faster and larger formation contributing to the heat of reaction. This heat cannot be differentiated from the heat of reaction of silica nanoparticles and calcium hydroxide as this

phenomenon does not happen in a system with calcium hydroxide and chelators containing oxalate ligands.

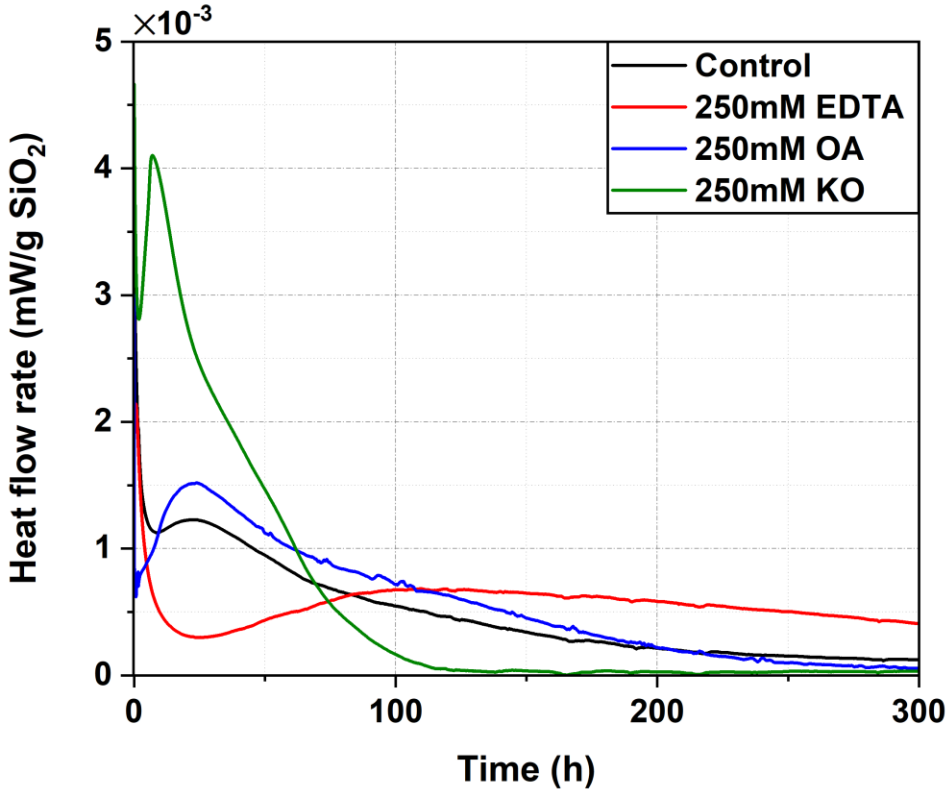

Figure 2.3 Heat flow of lime pastes with and without 250mM calcium chelators: ethylenediaminetetraacetic acid disodium salt dihydrate (EDTA), oxalic acid dihydrate (OA), and potassium oxalate monohydrate (KO).

In the lime paste with oxalate as chelating agent, after an initial intensified reaction in the system heat flow rate decreased to a lower extent than the control lime paste. This can be related to the large formation of calcium oxalate precipitating on the surface of undissociated calcium hydroxide and silica nanoparticles such that it restricts their further dissolution, and the progress of reaction will be diffusion controlled which is much slower than the reaction happening in the solution. Depending on the thickness of the precipitated calcium oxalate layer, there may be very small or no further reaction in the system as seen in the lime paste containing potassium oxalate.

Fig. 2.4 illustrates the cumulative heat of reaction between calcium hydroxide and silica nanoparticles in various systems with and without calcium chelators. According to Fig. 2.4, the cumulative heat of all lime pastes containing calcium chelators is higher than that of control lime system at later time (> 235h). With oxalate chelators, a portion of the reaction heat is associated with calcium oxalate precipitation at the early stage as discussed above. In the case of EDTA, however, higher heat of reaction is resulted from the higher quantity of reacted silica nanoparticles. Since agglomeration of silica nanoparticles is the main constraint limiting their reactivity in the systems, the prevention of forming large aggregates would make more nanoparticles available in the matrix, thereby resulting in a higher reaction degree and cumulative heat of reaction. Thus, by temporarily removing calcium ions during mixing and the very initial stage of reaction, the application of EDTA improved the reactivity of silica nanoparticles in the studied lime system.

To better compare the effect of calcium chelators on the reactivity of silica nanoparticles, reaction kinetics model was applied to estimate the ultimate reaction heat and reaction rate constant for each system (Table 2.2). Although the kinetics model well fitted the data for the simple $Ca(OH)_2$-SiO_2 system in the control lime paste, it does not fully capture the early-stage reaction kinetics for the systems with calcium chelators, suggesting more complex models are needed.

Nonetheless, the fitting parameters of the model were used for qualitatively comparing the ultimate heat. As presented in Table 2.2, the ultimate heat in all systems incorporating calcium chelators is higher than the ultimate heat of control lime system indicating that the removal of calcium ions during very initial stage of silica nanoparticles' reaction can be beneficial for their ultimate reactivity. Note that calcium removal strategy should be adopted together with a proper mixing practice to ensure well dispersion of silica nanoparticles within the system.

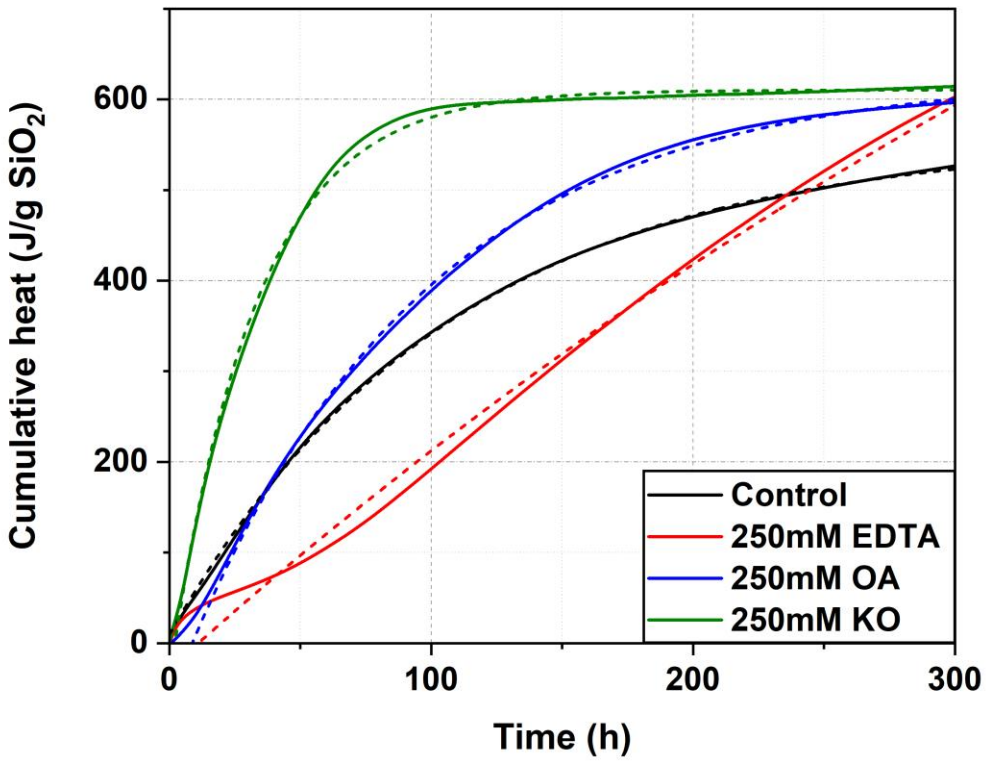

Figure 2.4 Cumulative heat of reaction between calcium hydroxide and silica nanoparticles. Dashed lines show the reaction kinetics model.

Table 2.2 Fitting parameters for the reaction kinetics model in $Ca(OH)_2$-SiO_2 system.

Mix	k (h^{-1})	H_o (J/g SiO_2)
Control	0.0094	547
Potassium oxalate (250mM)	0.0307	650
Oxalic acid (250mM)	0.0109	689
EDTA (50mM)	0.0040	992
EDTA (100mM)	0.0027	1241
EDTA (250mM)	0.0016	1648

As reflected in higher ultimate reaction heat (H_o) in Table 2.2, among all calcium chelators, EDTA ligand showed the best performance in terms of improving the reactivity of silica nanoparticles in lime-based matrix. On the other hand, EDTA lengthened the induction period, decelerating the reaction (lower rection rate constant k). This deceleration is largely due to a more pronounced induction period after EDTA is applied, as shown in Fig. 2.3. The removal of calcium ions from the solution by EDTA could limit C-S-H precipitation but allow the dissolution of silica nanoparticles to proceed, thereby increasing the concentration of dissolved silica species, especially near the nanoparticles. Upon depletion of EDTA molecules, the concentration of calcium ions increases suddenly, which can lead to thick C-S-H layers forming around the undissolved calcium hydroxide particles and silica nanoparticles. Such C-S-H layers would have a passivating effect decelerating further particle dissolution and reducing the overall reaction rate. A similar phenomenon was observed in cement-based materials incorporating EDTA (Thomas et

al. 1983). The passivating layer would eventually rupture due to osmotic process, leading to renewed $Ca(OH)_2$ and SiO_2 reaction and ending the induction period.

To further study the effect of EDTA concentration on the performance of silica nanoparticles in lime paste, EDTA at concentrations of 50mM and 100mM were tested. Fig. 2.5 and Fig 2.6 show the calorimetry test results on lime pastes incorporating different concentrations of EDTA. According to Fig. 2.5, increasing the concentration of EDTA prolonged the induction period and reduced the height of the main reaction peak. However, reaction proceeds at a higher heat flow rate at later times by increasing the EDTA dosage. This is confirmed by reaction kinetics modelling showing the ultimate heat of reaction was larger at higher concentration of EDTA while the reaction rate constant decreased (Table 2.2). As shown in Fig. 2.6, it is worth mentioning that despite the mismatch between the model and the calorimetry data at the initial stage of reaction, the model could effectively estimate the intersection between cumulative heat curves of lime systems with 50mM and 100mM EDTA. As presented in Table 2.3, the actual cumulative heat when the two heat curves intersect is 622 J/g SiO_2, while the model resulted in 608.3 J/g SiO_2. The difference is 2%, which is relatively low. As such, the model was used to estimate the time that cumulative heat curves cross each other, or the time at which higher reaction of silica nanoparticles was achieved, in the systems with EDTA. Results in Table 2.3 reveal that after around 533h from the beginning of reaction the cumulative heat in the lime paste with 250mM EDTA surpassed the cumulative heat in all systems containing EDTA as well as other systems studied herein. At this time, the cumulative heat of lime mixture incorporating 250mM EDTA is 909.1 J/g SiO_2 which is ca. 55% of the ultimate heat of reaction in this system.

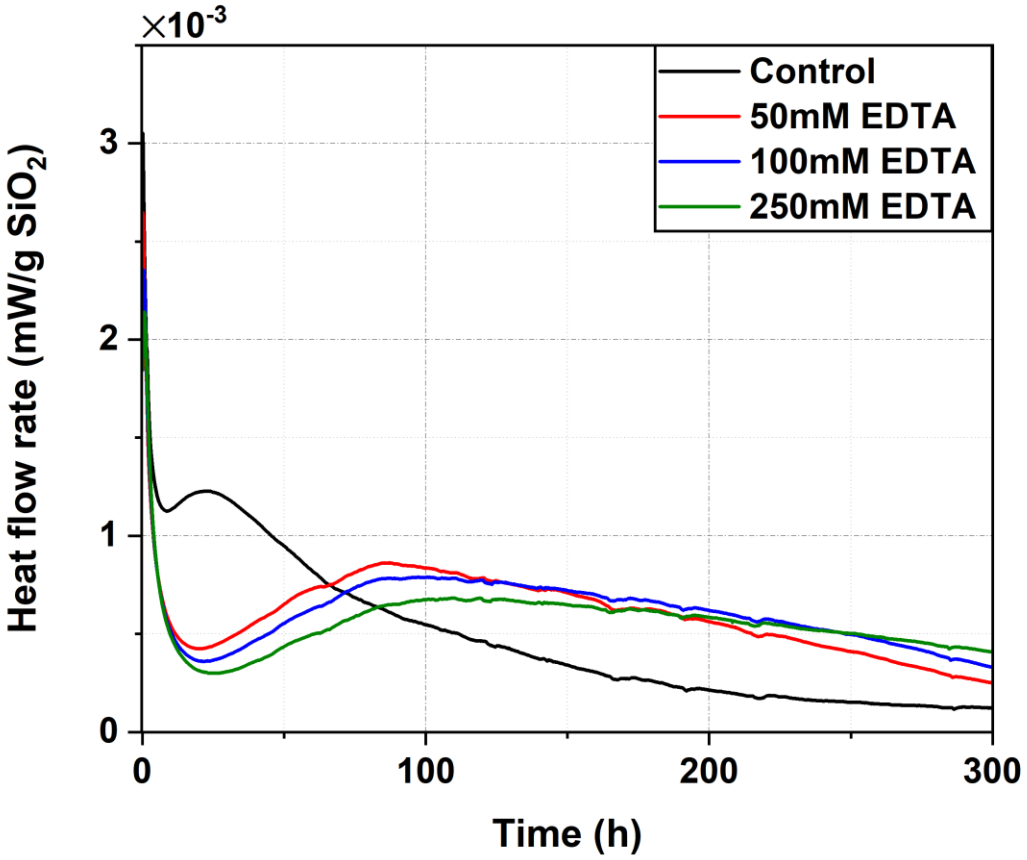

Figure 2.5 Heat flow rates of lime pastes with various concentrations of EDTA.

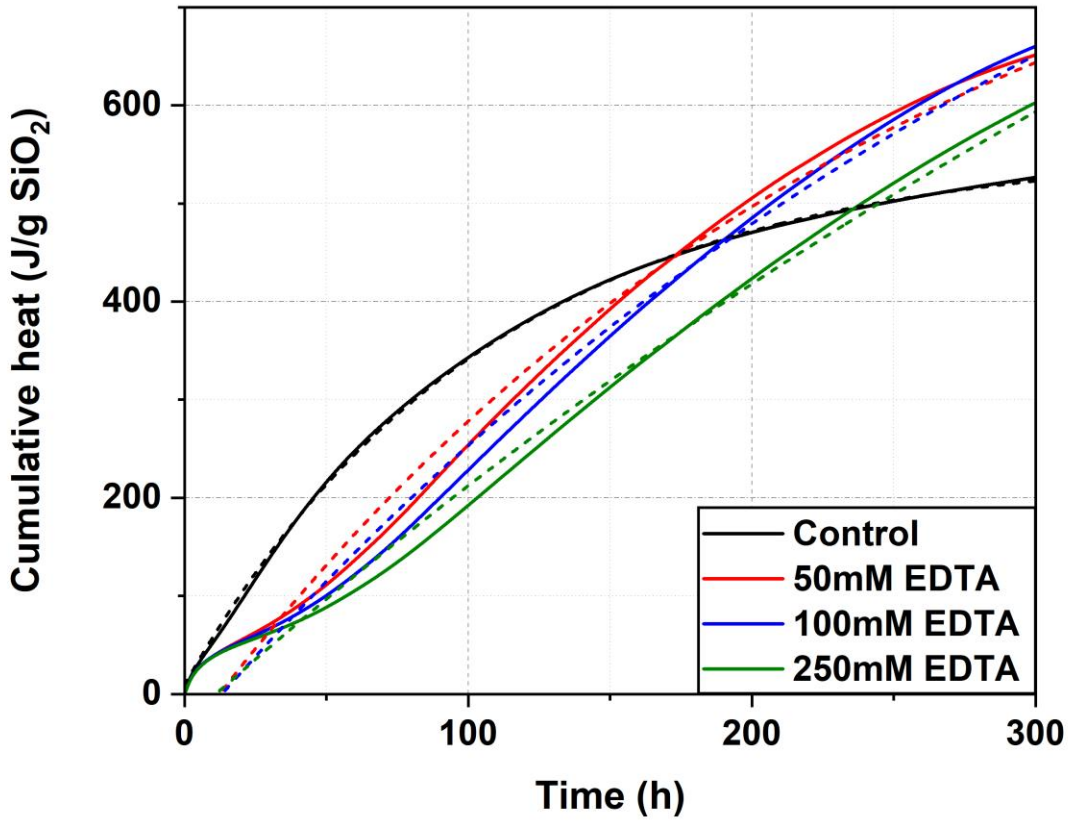

Figure 2.6 Cumulative heat of reaction of lime pastes with various concentrations of EDTA. Dashed lines show the reaction kinetics model.

Table 2.3 Estimation of cumulative heat curves intersection by the reaction kinetics model.

Intersecting curves	Intersection time (h)		Cumulative heat at intersection (J/g SiO_2)	
	Actual data	Model	Actual data	Model
50mM & 100mM EDTA	271.8	272.0	622.0	608.3
50mM & 250mM EDTA	NA	398.4	NA	741.1
100mM & 250mM EDTA	NA	532.8	NA	909.1

2.3.2.2 Thermogravimetry

Fig. 2.7 presents the results of TGA on the lime paste samples containing 50mM and 250mM at 7 and 28 days of reaction. According to Fig. 2.7, the consumed calcium hydroxide contents in the pastes containing 50mM and 250mM EDTA are 11% and 24%, respectively, less than that in the control lime paste. However, at 28 days, the consumed calcium hydroxide is 28% and 49% higher compared to the control paste for the mixtures with 50mM and 250mM EDTA, respectively. This observation is in agreement with calorimetry data, where the cumulative heat of control, 50mM, 250mM mixtures at 7 days is 442 J/g SiO_2, 436 J/g SiO_2, and 354 J/g SiO_2, respectively. Based on the reaction kinetics model, the cumulative heat for the aforementioned lime pastes is estimated to be 630 J/g SiO_2, 831 J/g SiO_2, and 920 J/g SiO_2, respectively, at 28 days. This implies that by increasing the concentration of EDTA, the quantity of consumed calcium hydroxide increases at 28 days. Note that TGA characterizations here focus on EDTA modified samples since EDTA shows the best efficacy in enhancing silica nanoparticle reactivity in lime systems. Also, the temperature ranges for the decomposition of calcium oxalate (product of calcium hydroxide and oxalate reaction) overlap with those of calcium hydroxide and calcium

carbonate (Fig. A.2 and A.3, Appendix A), making TGA results difficult to interpret for samples containing calcium chelators with oxalate ligand (i.e. potassium oxalate and oxalic acid).

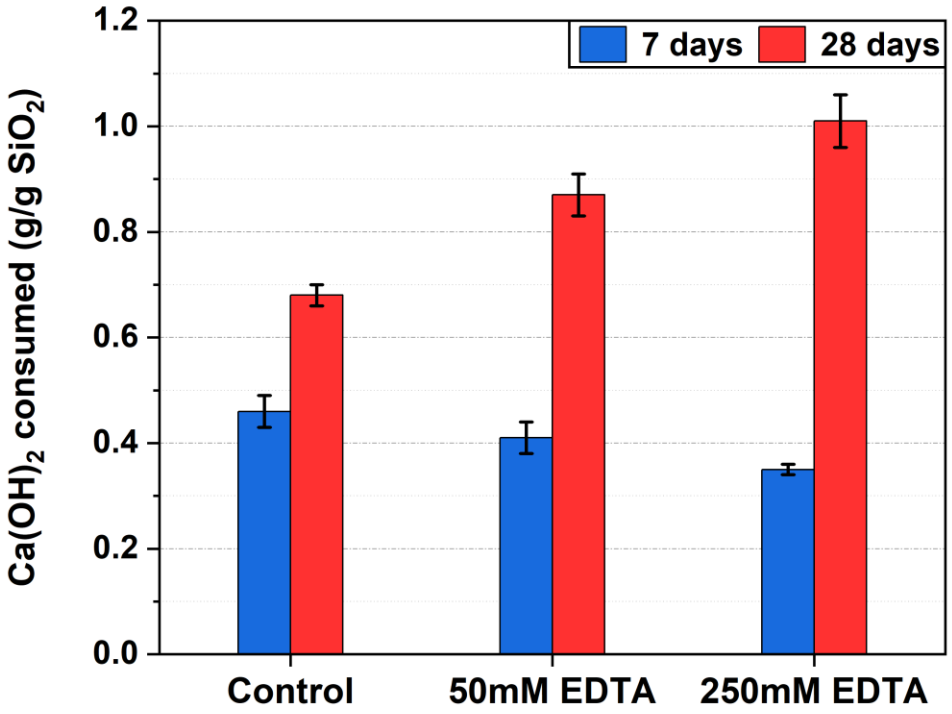

Figure 2.7 TGA results on lime paste samples with and without EDTA at 7 and 28 days of reaction.

2.3.3 Compressive strength

C-S-H resulted from the reaction between $Ca(OH)_2$ and SiO_2 possesses binding properties giving strength to the matrix (Moropoulou et al. 2004). Improving the reactivity of silica nanoparticles in lime-based materials should result in the production of more C-S-H and enhance the material's mechanical strength. As depicted in Fig. 2.8, utilization of calcium chelators indeed enhances the compressive strength of lime mortar samples. Moreover, the addition of EDTA produced the highest strength among samples with calcium chelators—50mM and 250mM EDTA improved the compressive strength by 270% and 390% comparing to the control lime mortar. Potassium oxalate and oxalic acid also showed modest improvements in the compressive strength at 39% and 29%, respectively. This validates the results of isothermal calorimetry and thermogravimetric tests and indicates that EDTA can effectively improve the reactivity of silica nanoparticles in lime-based composites and improve their mechanical properties. The compressive strength measurements are also in accordance with the thermal analysis data in implying potassium oxalate performs better than oxalic acid in terms of enhancement of silica nanoparticles reactivity in lime-based materials.

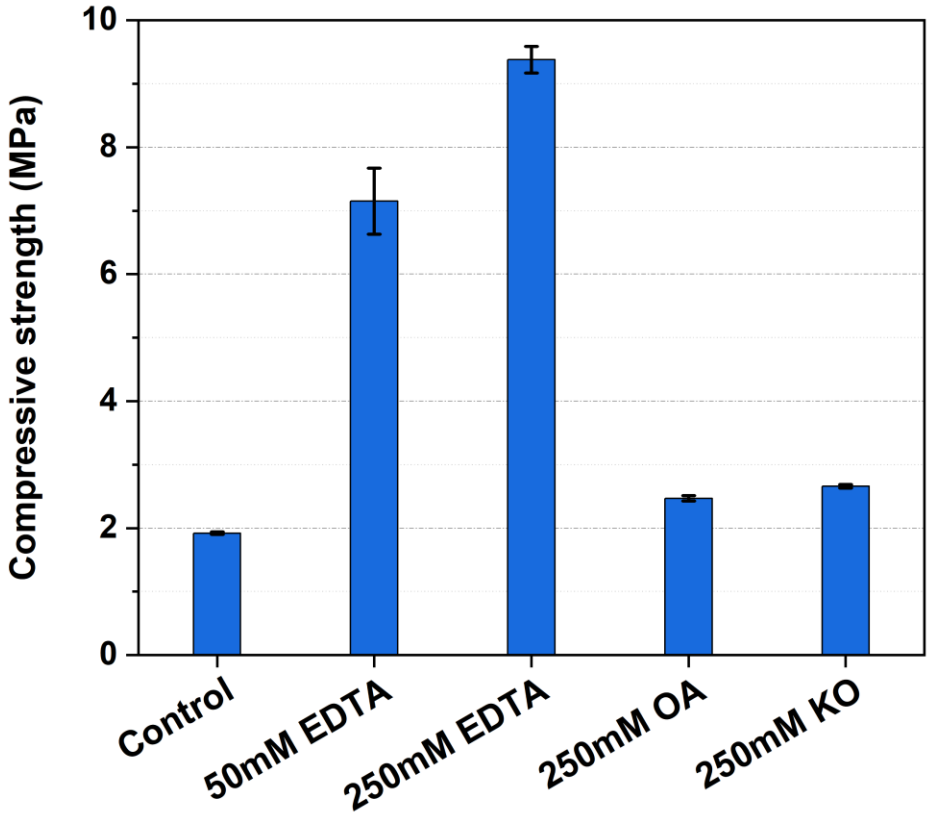

Figure 2.8 Results of compression test on lime mortars with and without calcium chelators.

2.4 Conclusions

The effect of temporary removal of calcium ions from the solution using calcium chelators on the reactivity of nanoparticles in the $Ca(OH)_2$-silica nanoparticles system was investigated. Based on the findings of this research, the following conclusions can be drawn:

1. Silica nanoparticles agglomerate when added into $Ca(OH)_2$ solution, which limits their reaction extent in lime systems. This can be mitigated by temporarily removing calcium ions from the solution during mixing time (i.e., very initial stage of reaction) using calcium chelators.
2. Isothermal calorimetry test showed adding calcium chelators to the $Ca(OH)_2$-silica nanoparticles system led to an increase in the reactivity of silica nanoparticles. Chelator with EDTA ligand initially decelerated the reaction between $Ca(OH)_2$ and SiO_2 but led to higher heat of reaction surpassing the control lime paste at later times. Increasing the concentration of EDTA to 250mM resulted in higher ultimate heat of reaction.
3. Calorimetry results suggested that the progress of reaction in the lime system was impeded by the addition of oxalate chelators which may be related to the formation of passivating calcium oxalate layers. Potassium oxalate, which elevates pH when added to $Ca(OH)_2$ solution, resulted in higher ultimate heat of reaction as compared to oxalic acid.
4. TGA results validated the calorimetry data indicating that EDTA improved the reactivity of silica nanoparticles. Consumption of calcium hydroxide at later time (28 days) increases with the EDTA concentration.
5. Compressive strength of the samples with chelators surpassed that of the control lime mortar. The lime mortar sample containing 250mM EDTA showed the highest

compressive strength, 390% higher than the control mortar, which is in accordance with the calorimetry analysis and TGA.

Chapter 3

Kinetics and apparent activation energies for reaction of silica nanoparticles with calcium hydroxide

3.1 Introduction

Lime is a versatile, easy-to-use material that is still widely used in environmental, asphalt, soil stabilization, and building construction (Zhang et al. 2011, Santoro et al. 1987, Mouillet et al. 2014, and Diamond et al. 1965). Limestone, dolomite, and chalk are common natural sources of lime because they mainly contain calcium carbonate. After calcination, the calcium carbonate generates quicklime. Quicklime may be processed to produce various lime products, including quicklime powder, hydrated lime powder, lime cream, and lime paste (Zhang et al. 2011). Lime has been extensively used in environmental applications, particularly acid wastewater treatment (Santoro et al. 1987). Lime, when used as an additive in asphalt, improves its durability and slows the chemical aging process of bitumen (Mouillet et al. 2014). Because most soils are essentially made of uncombined silica and various form of silicates, such as aluminosilicates in clays, lime is a suitable soil stabilizer. The chemical reaction of soil with lime produces cementitious compounds, principally hydrated calcium silicates and hydrated calcium aluminates. This response is the so-called pozzolanic reaction in the soil to create new cementitious nature, which is responsible for soil strength growth and stability (Diamond et al. 1965). In construction, the dominant application of lime is in grouts, mortars, roadbeds, and building foundations (Zhang et al. 2011, and Bras et al. 2012).

The science of nanostructured materials is rapidly evolving and will be used widely to produce various composites (Qing et al. 2006). The hydration, hardening, and durability of cement-based materials can be effectively improved using nanomaterials, particularly silica nanoparticles. The durability of materials made from lime can also be enhanced by incorporating silica nanoparticles (Luo et al. 2019). For example, a small quantity of silica nanoparticles can be used to make high-performance concrete by consuming the calcium hydroxide crystals that form at an early age at the interface between aggregate and hardened cement paste. This pozzolanic reaction creates an additional nanostructured substance in concrete for its major hydrate, calcium silicate hydrate gel (Qing et al. 2006). Although silica fume is another amorphous form of silica that is mainly composed of non-crystalline silica with a high specific surface area and falls under the category of highly pozzolanic materials, the research indicates that the pozzolanic reaction of silica fume at an early age is low. However, silica nanoparticles have much higher pozzolanic activity than silica fume and provide nucleation sites for the growth of calcium silicate hydrate gel (Qing et al. 2006, and Maddalena et al. 2019). Thermal analysis and apparent activation energy information are crucial for comprehending the time-dependent behavior of such cementitious systems (Sargam et al. 2021).

In a single reaction system, the apparent activation energy represents the potential energy barrier between reactants and products (Sargam et al. 2021). The apparent activation energy is also known as the least amount of energy necessary to start a chemical reaction (Liao et al. 2021). Because cement hydration is a temperature-sensitive reaction, the apparent activation energy is used to understand and analyze the cement hydration kinetics (Sargam et al. 2021, and Liao et al. 2021). The apparent activation energy is also frequently used to determine concrete maturity, heat generation, and equivalent age. It predicts temperature development in mass concrete constructions

(Sargam et al. 2021). The most used experimental technique for determining the apparent activation energy of cementitious materials is isothermal calorimetry. The exponential approach may be used to capture the heat rates at various temperatures, and the apparent activation energy can be calculated in accordance with the Arrhenius equation (Sargam et al. 2021, and Liao et al. 2021). Because the temperature significantly affects the cement hydration, high apparent activation energy indicates a temperature-sensitive reaction rate (Liao et al. 2021). The same activation energy might be produced in concrete by altering curing temperatures and periods. For instance, with the same apparent activation energy of 40 kJ/mol, a concrete specimen can be cured for 12 hours at 40 °C or 26 hours at 25 °C (Sargam et al. 2021).

In the current study, lime pastes were made with two types of silica nanoparticles with different specific surface areas and particle sizes. They were evaluated at various temperatures, including 30, 40, and 50 °C, with and without pH elevation. The specific surface areas for the coarse and fine silica nanoparticles are 90 and 300 m^2/g. Also, their average particle size is 34 and 9 nm, respectively. The isothermal calorimetric data of these lime systems were examined to determine the heat flow and corresponding cumulative heat released. Then, using an exponential approach, the reaction heat rates were calculated. The Arrhenius equation was later used to obtain the apparent activation energy. Additionally, the effect of employing disodium EDTA was evaluated and compared with experiments conducted without it.

3.2 Materials and methods

3.2.1 Materials

Calcium hydroxide and colloidal silica were used to make the lime pastes. Reagent-grade calcium hydroxide was used in white powder form with a purity of ≥ 95%. It was supplied by Alfa

Aesar. Two aqueous alkaline colloidal silica types were explored, namely, CB9 and CB30. Nouryon Chemicals, Marietta, GA, supplied them. They were available in a stabilized solution with sodium hydroxide. CB9 contains about 50% of solids by weight, whereas CB30 contains about 30% of solids by weight. CB9 nanoparticles are coarser than CB30. CB9 and CB30 have specific surface areas of 90 and 300 m^2/g, respectively. Also, their average particle size is 34 and 9 nm, respectively. Table 3.1 summarizes their technical characteristics.

Table 3.1 Technical data of the two types of colloidal silica used in this study.

Characteristics	CB9	CB30
Silica	50 wt.%	30 wt.%
Density	1.4 g/cm^3	1.2 g/cm^3
pH	9	10.5
Viscosity	15 cP	7 cP
Specific surface area	90 m^2/g	300 m^2/g
Average particle size	34 nm	9 nm

Ethylenediaminetetraacetic acid disodium salt dihydrate (EDTA) was used as a calcium chelating agent. It was obtained as a white granular powder in a reagent grade from Acros Organics. EDTA was dissolved in deionized water at the desired molarity and magnetically stirred for 24 hours. The solubility of EDTA in water can reach about 300mM (Davies et al. 2006).

3.2.2 Methods

3.2.2.1 Preparation of the lime paste mixtures

To explore the influence of the type of silica nanoparticles on pozzolanic reactivity, lime pastes containing coarse and fine colloidal silica nanoparticles were made. A weight ratio of 10 for calcium hydroxide to silica nanoparticles (C/S) was investigated. A constant liquid-to-solid weight ratio of 1.5 was used. This study explored three liquid solutions: 0.5M KOH, pre-dissolved 250mM EDTA chelator in denoised water, and pre-dissolved 250mM EDTA chelator in 0.5M KOH.

First, the bowl was loaded with the determined amount of calcium hydroxide. Then, the deionized water or the liquid solution was added. After that, the colloidal silica amount was added. The lime pastes were mixed using a vacuum mixer set to 450 rpm for four minutes. Table 3.2 shows the mix designs of lime pastes with and without EDTA and KOH.

3.2.2.2 Measurements of the heat of reaction of the lime pastes at different temperatures

The current investigation measured the heat generation rate of lime paste samples using an eight-channel TAM Air isothermal calorimeter. The experiments were conducted at three different temperatures: 30, 40, and 50 °C. Following mixing, the lime pastes were put into vials and securely sealed before being placed in the calorimetry instrument. After the testing time was finished, the heat flow and cumulative heat released were determined. For all measurements, the same sample preparation and testing method were employed. The values of cumulative heat released of reaction calculated based on the heat flow of two examined samples for each mixture were averaged and taken as a representative value.

Table 3.2 Mix designs of lime pastes for testing the activation energy

Mix	SiO_2	C/S	L/S	EDTA (mM)	KOH (mM)
Control CB9 w/o KOH	CB9	10	1.5	N/A	N/A
CB9 250mM EDTA w/o KOH	CB9	10	1.5	250	N/A
Control CB9 w/ KOH	CB9	10	1.5	N/A	500
CB9 250mM EDTA w/ KOH	CB9	10	1.5	250	500
Control CB30 w/o KOH	CB30	10	1.5	N/A	N/A
CB30 250mM EDTA w/o KOH	CB30	10	1.5	250	N/A
Control CB30 w/ KOH	CB30	10	1.5	N/A	500
CB30 250mM EDTA w/ KOH	CB30	10	1.5	250	500

3.2.2.3 Reaction rate and apparent activation energy

The relationship between the reaction rate and the apparent activation energy is formulated by the Arrhenius equation (Eq.3.1), which was applied and found applicable for calculating the apparent activation energy of cement-based materials (Liao et al. 2021).

$$k = A \cdot e^{-\frac{E_a}{RT}} \quad \text{(Eq.3.1)}$$

Where k is the temperature-dependent reaction rate, A is the pre-exponential factor, E_a is the apparent activation energy, T is the temperature (K), and R is the universal gas constant. The value of R is taken as 8.314 J/ (mol. K). Another equation could be obtained (Eq.3.2) by taking the ln on both sides of the Arrhenius equation (Eq.3.1) and denoting k_c as the reaction rate at different testing temperatures, T_c. Also, Eq.3.3 was derived in the same manner where k_{ref} is the reference reaction rate at the reference testing temperature, T_{ref}. By subtracting Eq.3.3 from Eq. 3.2, a linear relationship for the reaction rate versus temperature data exists (Eq.3.4). Using eq. 3.4, an Arrhenius plot with a slope equal to E_a/R can be fitted and used to determine the apparent activation energy of the reaction in kJ/mol (Liao et al. 2021).

$$ln(k_c) = ln(A) - \frac{E_a}{RT_c} \quad \text{(Eq.3.2)}$$

$$ln(k_{ref}) = ln(A) - \frac{E_a}{RT_{ref}} \quad \text{(Eq.3.3)}$$

$$ln\left(\frac{k_c}{k_{ref}}\right) = -\frac{E_a}{R}\left(\frac{1}{T_c} - \frac{1}{T_{ref}}\right) \quad \text{(Eq.3.4)}$$

Further, the reaction rate is often calculated from an exponential model (Eq.3.5). It is used to fit the cumulative heat released by cement-based materials (Sargam et al. 2021, and Liao et al. 2021).

$$H(t) = H_u \cdot e^{-\left(\frac{\tau}{t}\right)^{\beta}} \quad \text{(Eq.3.5)}$$

Where H(t) is the cumulative heat evolved (J/g) at time t, H_u is the ultimate cumulative heat released (J/g), and τ is the reaction time parameter (h), β is the reaction shape parameter. The rate of reaction, k (h^{-1}), is equal to the reciprocal of τ (Liao et al. 2021). A larger τ implies a longer delay in the response (Sargam et al. 2021).

In this study, the apparent activation energy of the reaction of lime with silica nanoparticles was calculated by measuring the reaction rates at different temperatures, including 30, 40, and 50 °C. The reference temperature was chosen to be 30 °C. An Arrhenius plot of the reaction rate versus temperature measurements was created for each lime mixture using Eq. 3.4. An estimate of the apparent activation energy was calculated from the slope of the linear fit.

3.3 Results and discussions

3.3.1 Cumulative heat released at different temperatures

The cumulative heat-released curves for all eight mixtures tested at three different curing temperatures, 30, 40, and 50 °C (a total of 24 mixtures), are shown in Fig. 3.1 to Fig. 3.8. The data suggest that the reaction accelerates at higher temperatures. A similar observation was reported in the literature (Liao et al. 2021). This phenomenon might be explained by the rapid dissolution of silica nanoparticles caused by heating energy, resulting in the formation of the heavier C-S-H layers sooner. When the temperature was increased from 30 to 50 °C, the cumulative heat of the

reaction was considerably increased from 146 to 662 J/ g SiO_2 for CB9 lime paste mixture with 250mM EDTA after 50 hours of response (Fig. 2). In contrast to the lime pastes with CB30, increasing the temperature in each case with CB9 resulted in higher or equivalent accumulated heat.

Furthermore, the findings from the cumulative curves show that finer silica nanoparticles (CB30) respond more quickly than the coarse one (CB9). At 30 °C, Figs. 3.1 for control CB9 and Fig. 3.5 for control CB30 show that the CB9 mixture pursued the reaction for a longer period of time than the CB30. Still, after a very fast reaction of CB30, the reaction ended sooner with higher cumulative heat (≈ 140 J/ g SiO_2 more than CB9) but with no further response — two reasons for that. The first reason is agglomeration. The finer nanoparticles, the larger the agglomerates are formed (Khaloo et al. 2016). This agglomeration decelerates the pozzolanic activity, where the first layer of agglomerates will be dissolved in the saturated $Ca(OH)_2$ solution. Then, the beneath layers will be dissolved consecutively until getting to the core of the agglomerate. The other reason is the perception of dense C-S-H. This thick C-S-H prevents water molecules from getting to the layer of nanoparticles underneath the C-S-H. Because water molecules (hydroxyl ions) need to attack the surface of silica nanoparticles, then dissolve them to release the silicon ions for reaction, the thick C-S-H is hypothesized as the main reason for not obtaining a further response from the finer silica nanoparticles. Nonetheless, the control CB30 mixture produced higher cumulative heat than the control CB9 at 30°C reaction temperature

Based on the results of CB9 (Fig. 3.2), the calcium complexing agent, EDTA, showed higher cumulative heat released compared to the control CB9 mixture (Fig. 3.1). The same observation was noted for CB30 (Fig. 3.5 and Fig. 3.6). This finding indicates better dispersion of silica nanoparticles and improved pozzolanic reactivity in lime pastes. This research demonstrates

comparable effects to a previous study, which revealed that using EDTA produced thicker C-S-H layers (Thomas et al. 1983). However, the effect of EDTA on the dispersion was more pronounced for the coarser nanoparticles, CB9, than the finer one, CB30, and less effective with elevated pH cases (Fig. 3.4 and Fig. 3.8).

The hypothesis with pH elevation (using 0.5M KOH solution in the current study) is that the agglomeration of nanoparticles is more severe when both KOH and $Ca(OH)_2$ are offered in the pore solution (Reches et al. 2018). However, at this high pH (>9), the dissolution of amorphous silica increases exponentially (Ayral et al. 2006). Because of that, a higher amount of silica is dissolved with pH elevation, producing more C-S-H. So, the effect of agglomeration in high pH could be unnoticed because more silicon ions dissolution leads to the faster reaction of these silicon ions with calcium and hydroxyl ions. More cumulative heat was released from CB9 mixtures at elevated pH (Fig. 3.3) compared to the control CB9 mixture (Fig. 3.1). However, less cumulative heat was released from CB30 mixtures (Fig. 3.7) compared to the control CB30 mixtures (Fig. 3.5). This could be due to the thick formed C-S-H layer from the very fast dissolution of silicon ions and the rapid reaction of CB30 in the lime mixtures.

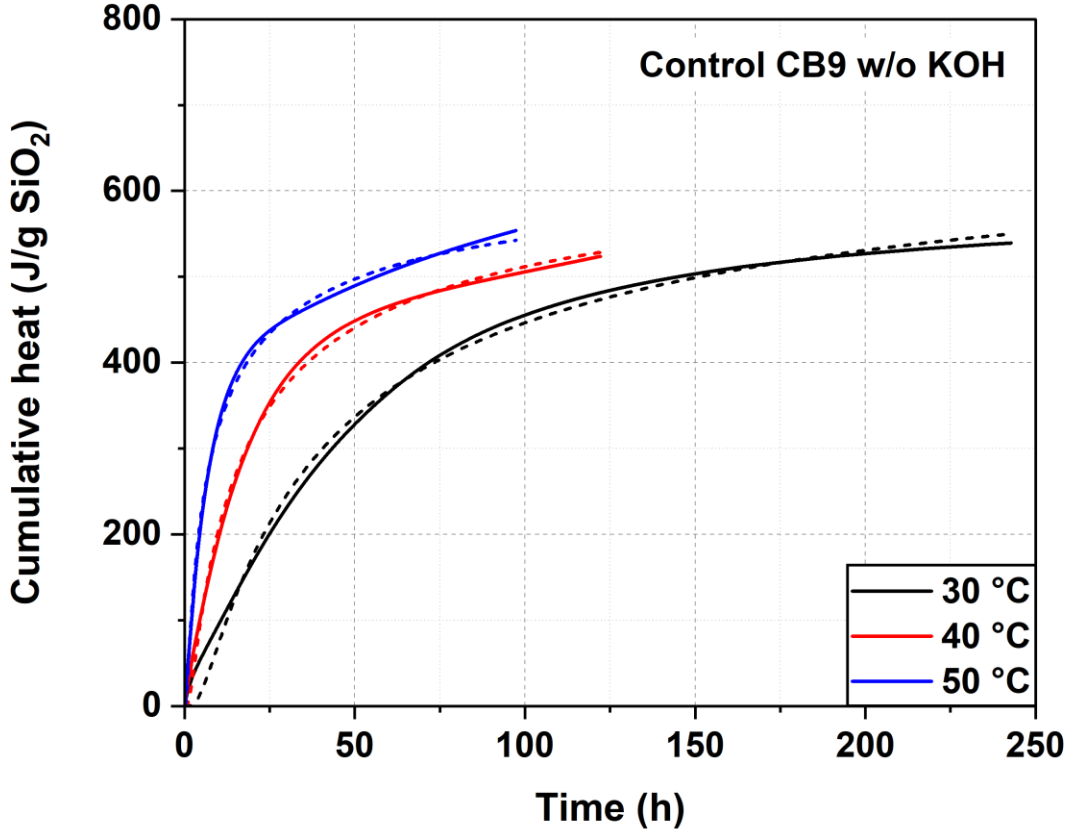

Figure 3.1 Cumulative heat released at different temperatures for the control lime mixture containing CB9 without KOH. Dashed lines show the reaction kinetics model.

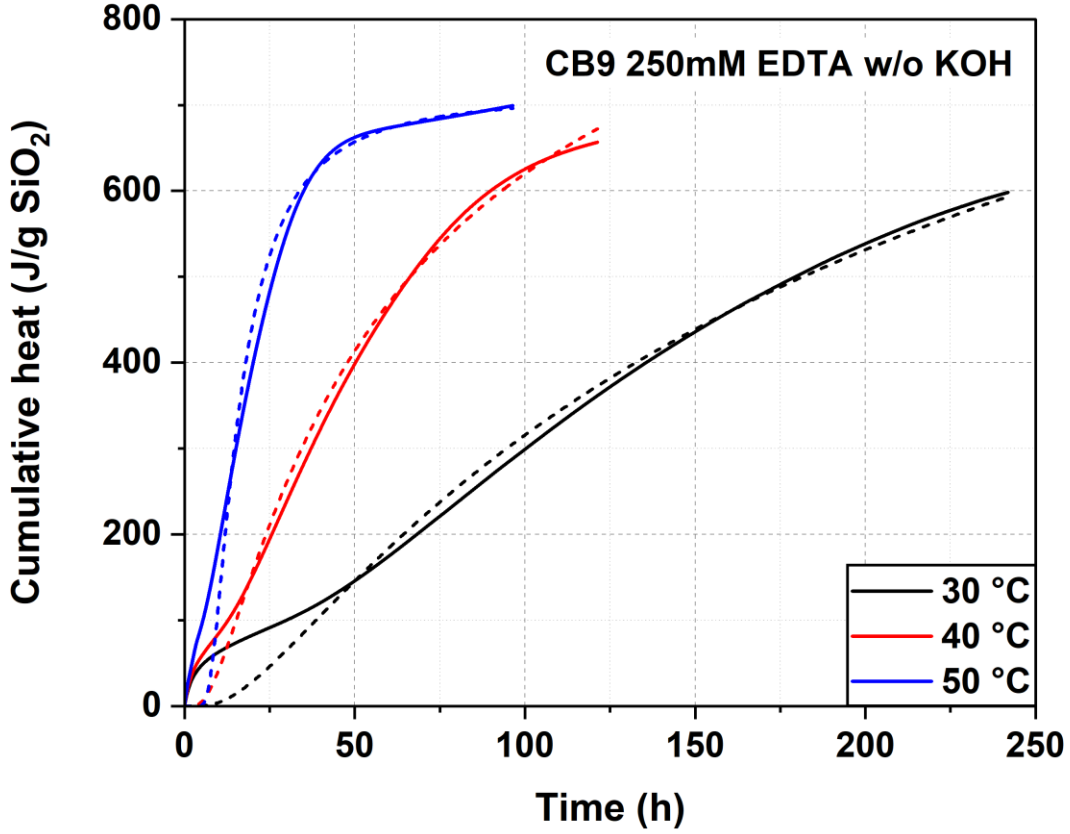

Figure 3.2 Cumulative heat released at different temperatures for the lime mixture containing CB9 with 250mM EDTA and without KOH. Dashed lines show the reaction kinetics model.

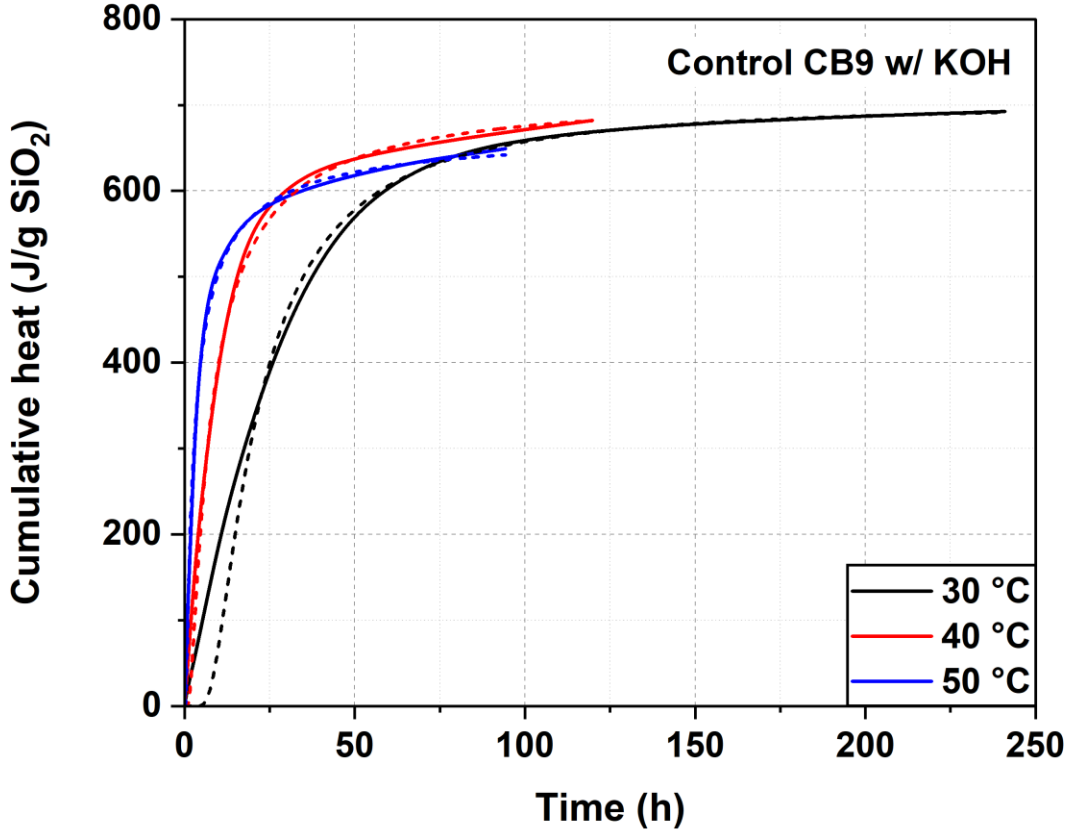

Figure 3.3 Cumulative heat released at different temperatures for the lime mixture containing CB9 with KOH. Dashed lines show the reaction kinetics model.

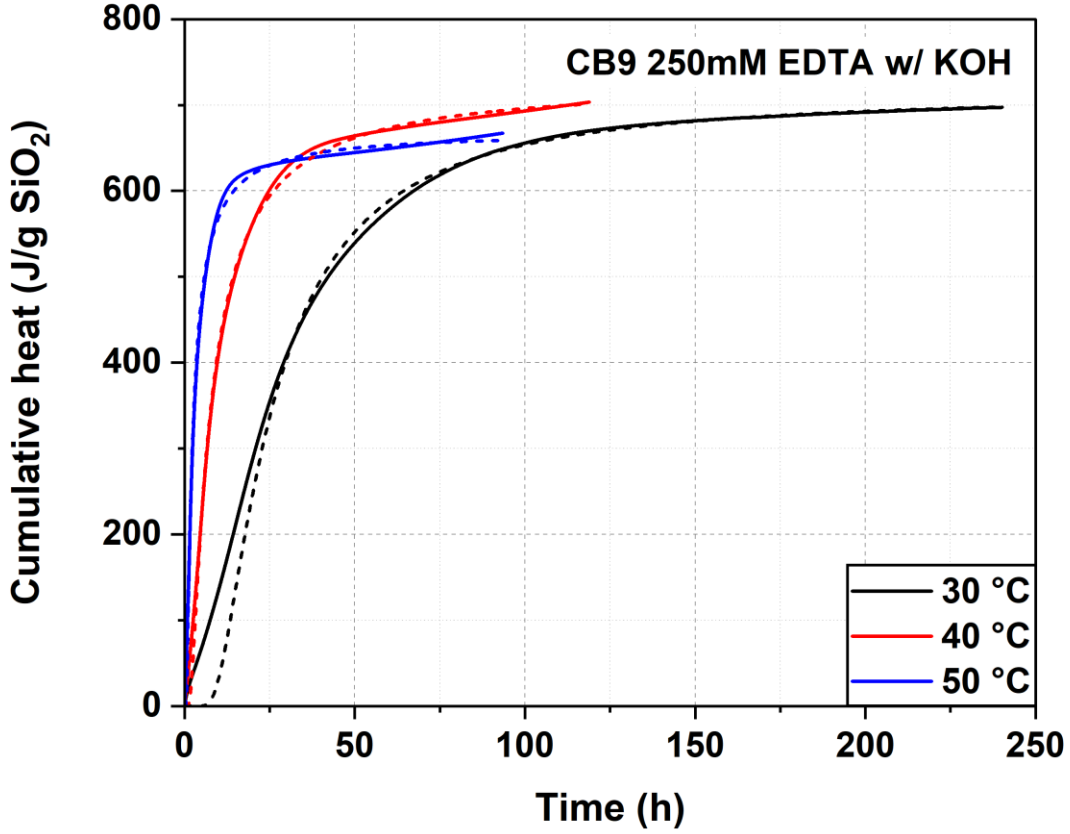

Figure 3.4 Cumulative heat released at different temperatures for the lime mixture containing CB9 with 250mM EDTA and KOH. Dashed lines show the reaction kinetics model.

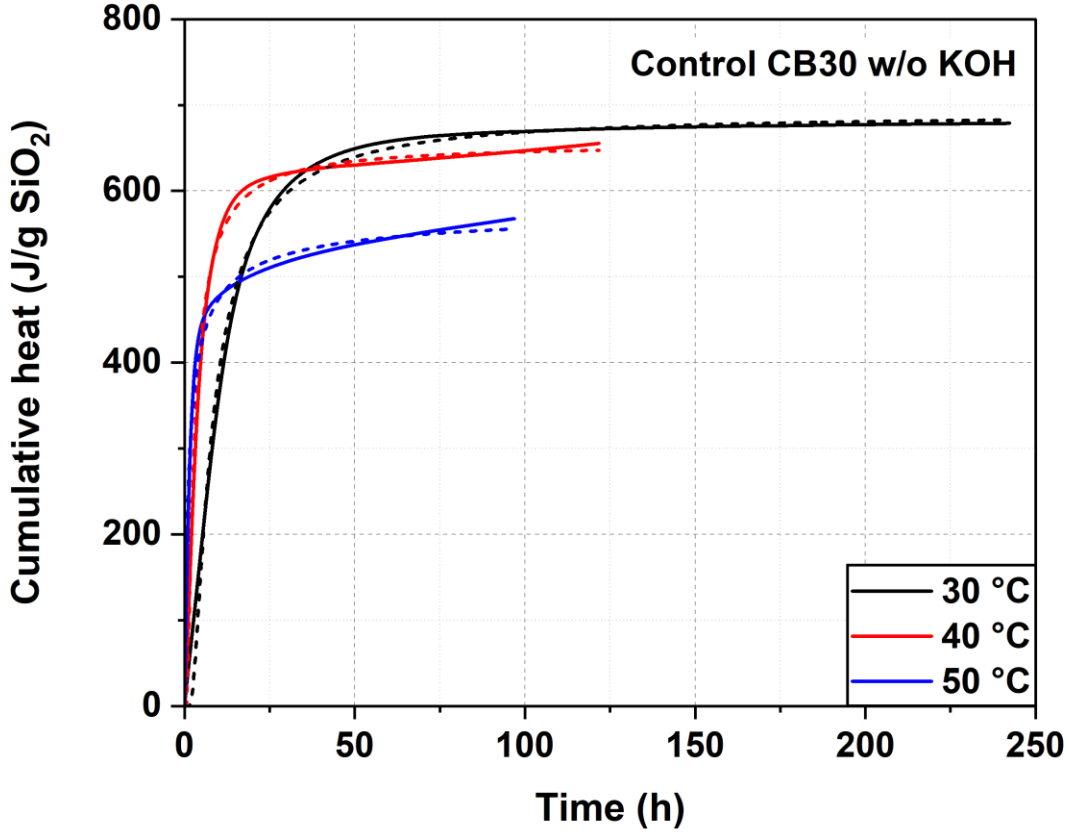

Figure 3.5 Cumulative heat released at different temperatures for the control lime mixture containing CB30 without KOH. Dashed lines show the reaction kinetics model.

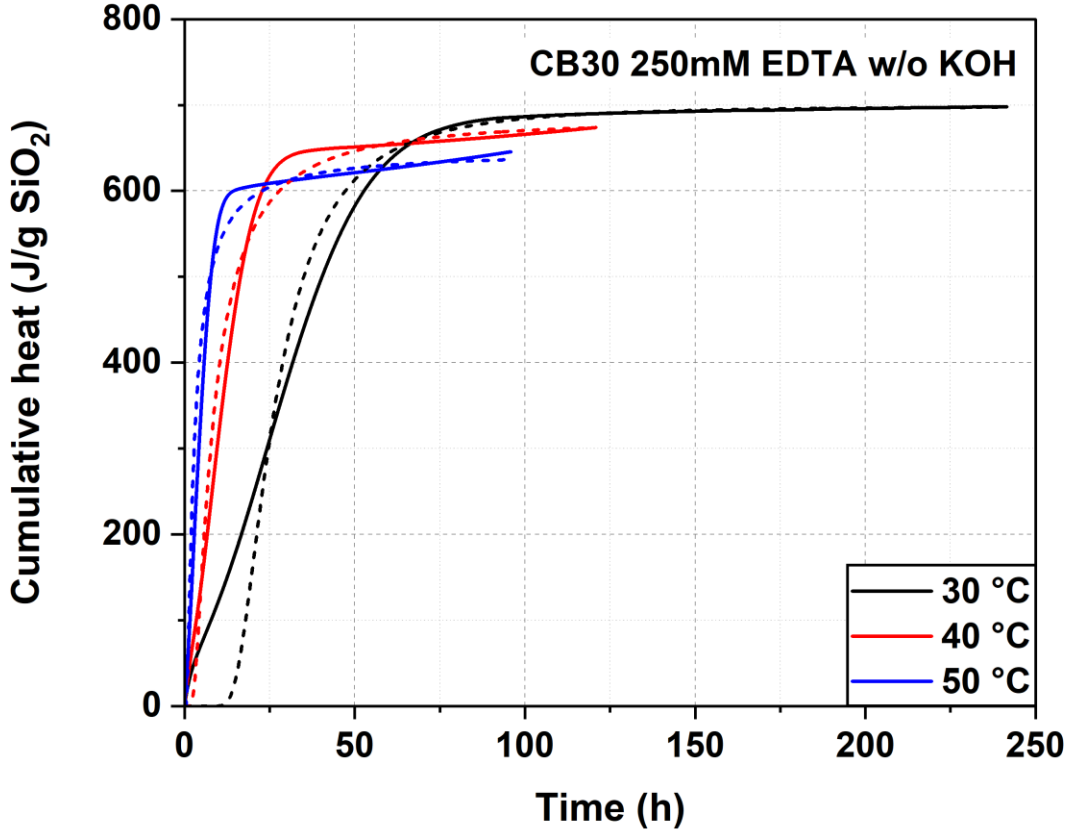

Figure 3.6 Cumulative heat released at different temperatures for the lime mixture containing CB30 with 250mM EDTA and without KOH. Dashed lines show the reaction kinetics model.

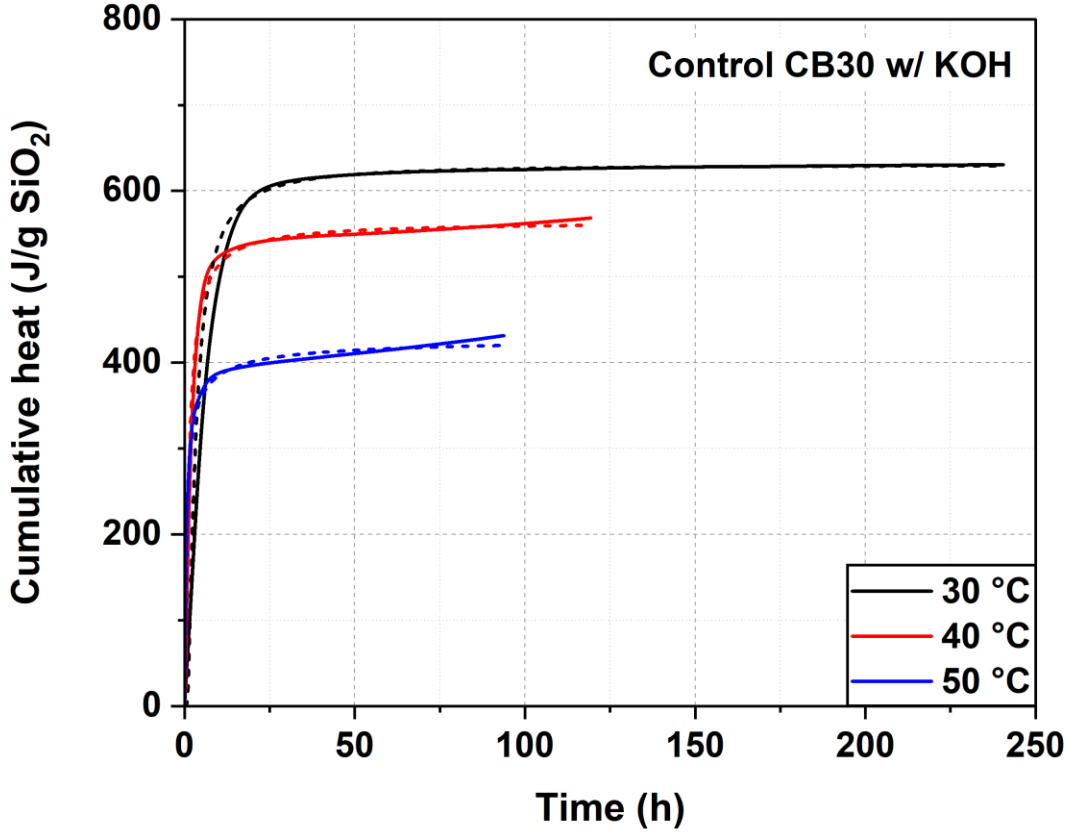

Figure 3.7 Cumulative heat released at different temperatures for the lime mixture containing CB30 with KOH. Dashed lines show the reaction kinetics model.

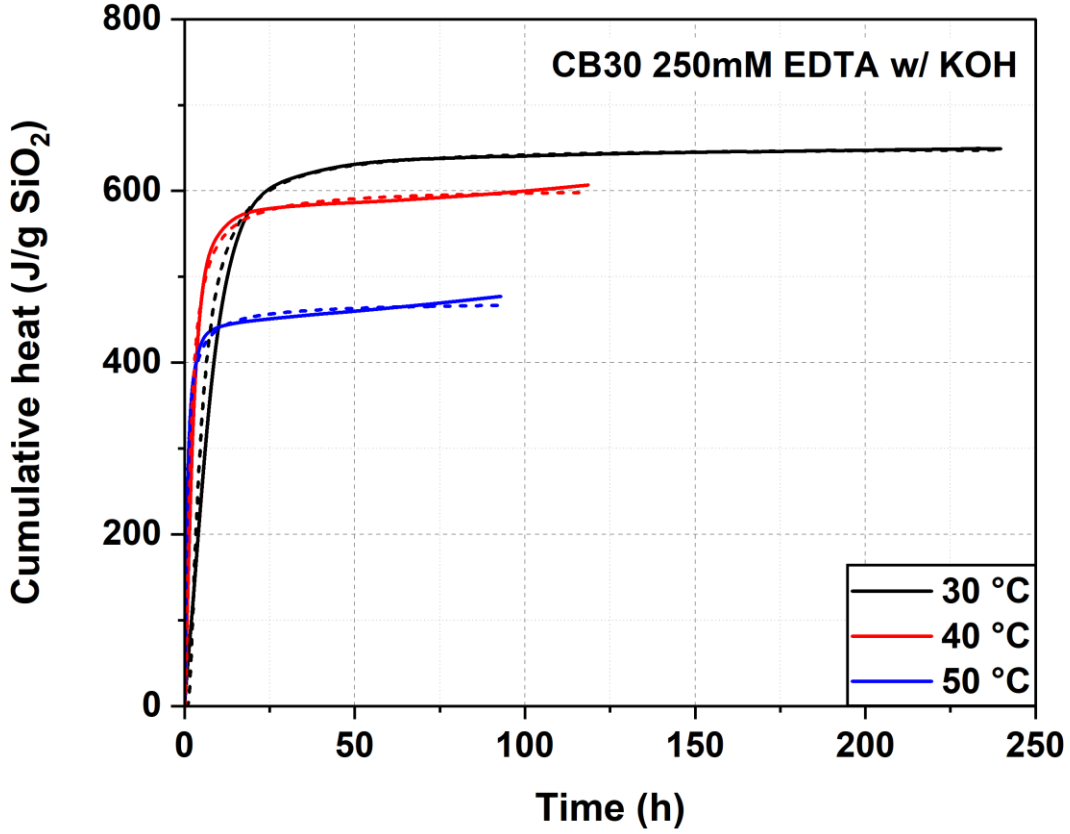

Figure 3.8 Cumulative heat released at different temperatures for the lime mixture containing CB30 with 250mM EDTA and KOH. Dashed lines show the reaction kinetics model.

3.3.2 Reaction kinetics and apparent activation energies

Tables 3.3 to 3.8 illustrate the reaction kinetics for all eight mixtures tested at three different curing temperatures, 30, 40, and 50 °C (a total of 24 mixtures). Each mixture showed unique reaction kinetics. However, it could be observed that increasing the curing temperature led to a faster reaction. The CB9 mixture with 250mM EDTA had τ values of 227 and 13.5 hours at 30 and 50 °C, respectively (Tables 3.3 and 3.5). The reaction at 30 °C was considerably slower since a larger τ donates a prolonged response (Sargam et al. 2021).

According to the results of the reaction kinetics, the EDTA retarding effect was not apparent in most of the cases when 0.5M KOH elevated the pH. In this observation, it is a reasonable conclusion that the retardation effect of EDTA was not present due to an accelerated reaction between the very fast dissolution of silica nanoparticles and $Ca(OH)_2$ in the elevated pH solution. For instance, at the elevated pH, the CB9 mixtures which was tested at 30 °C with or without EDTA generated an equivalent cumulative heat of 697 and 692.5 J/ g SiO_2, respectively (Fig. 3.3 and Fig. 3.4).

The calorimetric information shown in Tables 3.3 to 3.8 was used to compute the apparent activation energy (E_a) from the slope of the best-fitting line of Eq. 3.4 (Fig. B.1 to Fig. B.2, Appendix B). The exponential model perfectly fits the experimental data with an approximate R^2 of 1. The control CB9 mixture had the lowest E_a of 72 KJ/mol among all the samples evaluated in this investigation (Table 3.9). The E_a was increased to 114 KJ/mol when 250mM EDTA was added to the CB9 mixture (the highest recorded in this study). The influence of elevated pH solution for CB9 (Fig. 3.9) and CB30 (Fig. 3.10) on the E_a values was not similar, showing higher E_a obtained for the control CB9 mixture in elevated pH solution compared to that without, which in contrast to the case of CB30.

Table 3.3 Reaction kinetics determined from the exponential method for CB9 mixtures at 30 °C.

Mix	T = 30 °C				
	H_u (J/g SiO_2)	τ (h)	β	k (h^{-1})	R^2
Control CB9 w/o KOH	700.644	32.069	0.700	0.031	0.995
CB9 250mM EDTA w/o KOH	1555.961	226.791	0.570	0.004	0.986
Control CB9 w/ KOH	704.034	17.258	1.525	0.058	1.000
CB9 250mM EDTA w/ KOH	713.866	20.783	1.548	0.048	1.000

Table 3.4 Reaction kinetics determined from the exponential method for CB9 mixtures at 40 °C.

Mix	T = 40 °C				
	H_u (J/g SiO_2)	τ (h)	β	k (h^{-1})	R^2
Control CB9 w/o KOH	667.642	12.834	0.645	0.078	0.996
CB9 250mM EDTA w/o KOH	1145.988	51.325	0.731	0.019	1.000
Control CB9 w/ KOH	715.453	5.829	1.005	0.172	0.992
CB9 250mM EDTA w/ KOH	727.406	5.850	1.100	0.171	0.996

Table 3.5 Reaction kinetics determined from the exponential method for CB9 mixtures at 50 °C.

Mix	T = 50 °C				
	H_u (J/g SiO_2)	τ (h)	β	k (h^{-1})	R^2
Control CB9 w/o KOH	648.004	5.421	0.598	0.184	0.996
CB9 250mM EDTA w/o KOH	712.237	13.498	1.923	0.074	1.000
Control CB9 w/ KOH	673.995	2.090	0.793	0.478	0.997
CB9 250mM EDTA w/ KOH	668.575	1.846	1.080	0.542	0.995

Table 3.6 Reaction kinetics determined from the exponential method for CB30 mixtures at 30 °C.

Mix	T = 30 °C				
	H_u (J/g SiO_2)	τ (h)	β	k (h^{-1})	R^2
Control CB30 w/o KOH	689.716	6.507	1.267	0.154	0.992
CB30 250mM EDTA w/o KOH	699.022	23.077	2.625	0.043	1.000
Control CB30 w/ KOH	630.712	2.516	1.339	0.398	1.000
CB30 250mM EDTA w/ KOH	650.158	3.751	1.334	0.267	1.000

Table 3.7 Reaction kinetics determined from the exponential method for CB30 mixtures at 40 °C.

Mix	T = 40 °C				
	H_u (J/g SiO_2)	τ (h)	β	k (h^{-1})	R^2
Control CB30 w/o KOH	655.020	2.257	1.115	0.443	0.993
CB30 250mM EDTA w/o KOH	685.147	6.688	1.415	0.150	0.978
Control CB30 w/ KOH	564.450	0.958	1.003	1.043	0.986
CB30 250mM EDTA w/ KOH	603.213	1.283	1.060	0.780	0.987

Table 3.8 Reaction kinetics determined from the exponential method for CB30 mixtures at 50 °C.

Mix	T = 50 °C				
	H_u (J/g SiO_2)	τ (h)	β	k (h^{-1})	R^2
Control CB30 w/o KOH	584.349	0.835	0.629	1.198	0.981
CB30 250mM EDTA w/o KOH	645.959	2.219	1.119	0.451	0.959
Control CB30 w/ KOH	430.856	0.384	0.668	2.601	0.974
CB30 250mM EDTA w/ KOH	471.646	0.474	0.864	2.111	0.981

Table 3.9 Apparent activation energies estimated based on the rate of reaction.

Mix	E_a (kJ/mol)	R^2
Control CB9 w/o KOH	72.39	1.0000
CB9 250mM EDTA w/o KOH	114.93	0.9999
Control CB9 w/ KOH	85.96	1.0000
CB9 250mM EDTA w/ KOH	98.62	0.9999
Control CB30 w/o KOH	83.63	1.0000
CB30 250mM EDTA w/o KOH	95.39	0.9998
Control CB30 w/ KOH	76.49	0.9999
CB30 250mM EDTA w/ KOH	84.26	0.9999

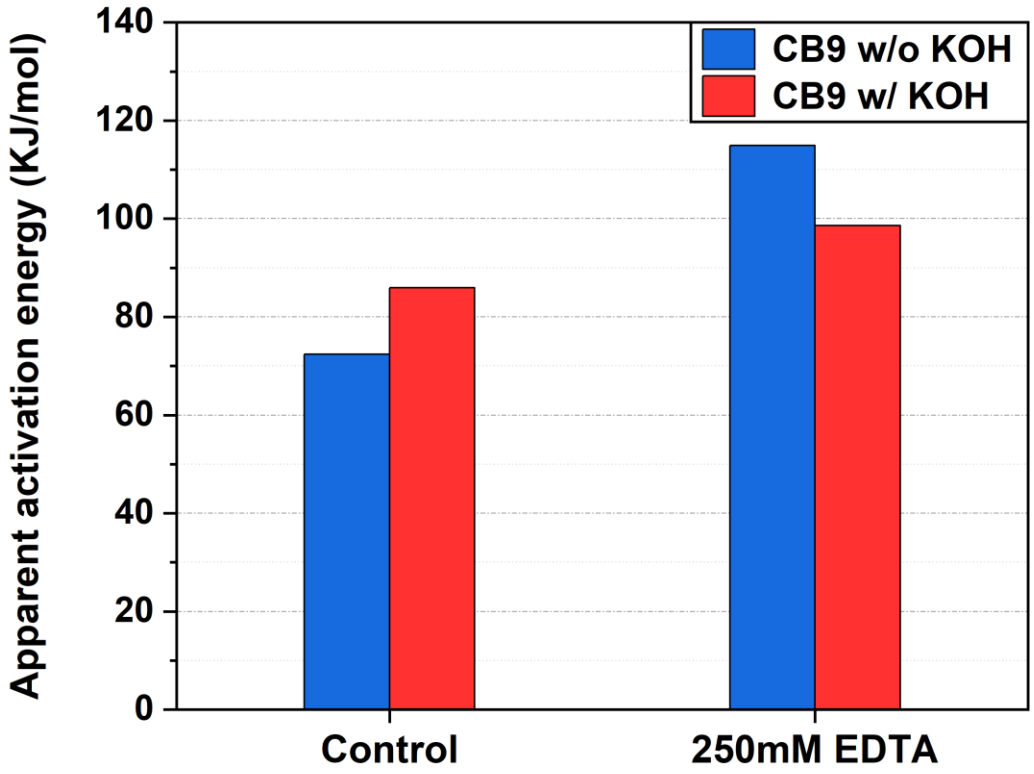

Figure 3.9 Apparent activation energy as determined by the exponential method for the lime mixture containing CB9 with and without 250mM EDTA and KOH.

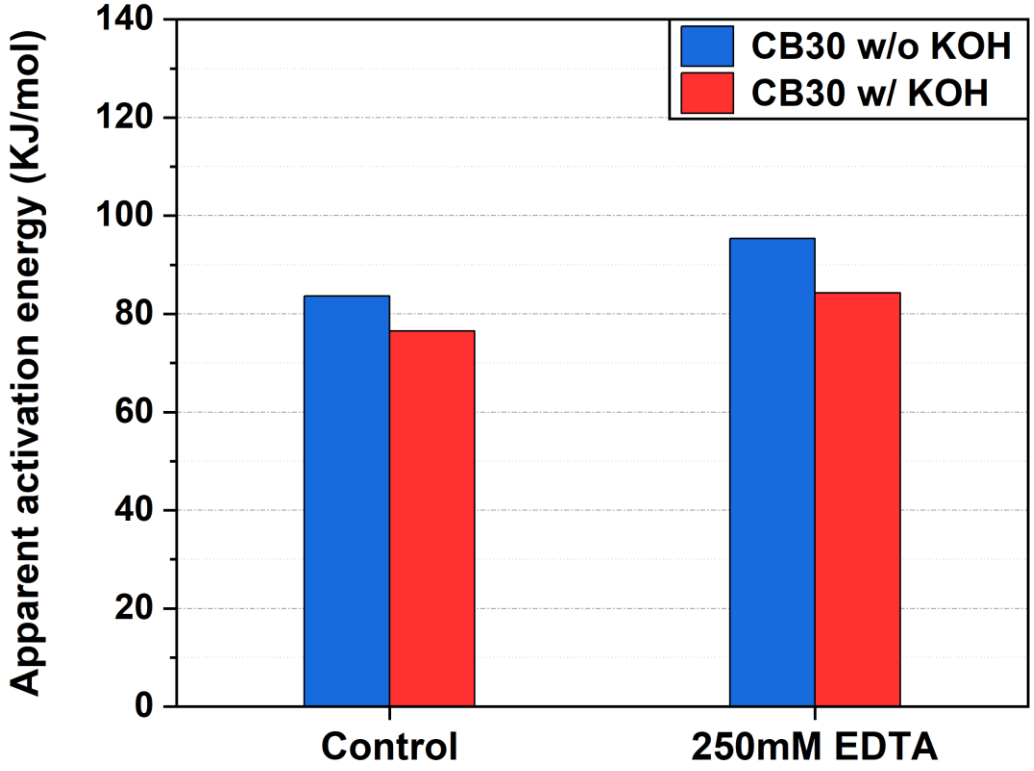

Figure 3.10 Apparent activation energy as determined by the exponential method for the lime mixture containing CB30 with and without 250mM EDTA and KOH.

3.4 Conclusions

The reaction kinetics and apparent activation energy of lime pastes containing silica nanoparticles were investigated. Based on the findings of this research, the following conclusions can be drawn:

1. The reaction accelerated at higher temperatures. As measured after 50 hours of response for the CB9 lime pastes with 250mM EDTA, the cumulative heat of the reaction considerably increased from 146 to 662 J/g SiO_2 when the temperature was elevated from 30 to 50 °C.
2. When the KOH offered the high pH, the EDTA retarding effect was not noticeable in most of the tested cases. For example, the CB9 mixture evaluated at 30 °C with or without EDTA produced almost an equal cumulative heat of 697 and 692.5 J/g SiO_2, respectively.
3. The reaction at 30 °C was slower than at elevated temperatures (40 and 50 °C). The CB9 mixture with 250mM EDTA had τ values of 227 and 13.5 hours at 30 and 50 °C. Larger τ donates prolonged response.
4. The exponential model used to compute the apparent activation energy perfectly fits the calorimetric data with an approximate R^2 of 1.
5. The control CB9 mixture had the lowest E_a of 72 KJ/mol among all the samples evaluated. The E_a was increased to 114 KJ/mol when 250mM EDTA was added, the highest recorded in this study.
6. The influence of elevated pH solution for CB9 and CB30 on the E_a values was not similar, showing higher E_a obtained for the control CB9 mixture in elevated pH solution compared to that without, which in contrast to the case of CB30.

Summary and concluding remarks

Silica nanoparticles can increase the performance of cementitious materials producing high strength composites. However, challenges with agglomeration affect their proper dispersion. In aqueous solutions, silica nanoparticles coagulate upon the adsorption of calcium ions which reduces the reactivity of these particles in calcium-rich media. To achieve full incorporation and fully reacting SiO_2 particles, an economical and effective dispersion technique is required to resolve the issue of silica nanoparticles agglomeration. Temporary removal of calcium ions from the solution, especially at the very early stage of the reaction (e.g. during mixing) can reduce the possibility of the agglomeration of these nanoparticles leading to improving their reactivity.

This study explored the reactivity, reaction kinetics, and apparent activation energy of silica nanoparticles in the lime system in relation to the removal of calcium ions from the solution using calcium chelators.

The average particle size of silica nanoparticles in saturated calcium hydroxide solution decreased with addition of the disodium salt of EDTA, a calcium ion chelator, indicating fewer agglomerates as compared to the calcium hydroxide solution without EDTA. Also, the isothermal calorimetric data showed that EDTA chelating agent initially slowed the reaction between silica nanoparticles and calcium hydroxide but eventually produced a more significant heat of reaction than the control lime paste. Furthermore, the lime mortar with 250mM EDTA had the maximum compressive strength, 390% more than the control mortar. Moreover, the consumption of calcium hydroxide increases with the EDTA concentration over time (28 days).

Besides, the exponential model used to estimate the apparent activation energy perfectly fits the calorimetric data of lime pastes. Also, the data collected at different curing temperatures

indicated that at a higher temperature, the reaction accelerated. The highest recorded apparent activation energy in this study—114 KJ/mol—occurred when 250mM EDTA was added to the lime system containing the coarser type of silica nanoparticles (CB 9) without pH elevation. Still, for the samples with pH elevation, the apparent activation energy values were seen to be higher in mixtures with EDTA compared to those without it. Despite having different silica nanoparticle types (CB9 and CB30), pH levels, and the presence or absence of EDTA, three mixtures produced equivalent cumulative heat of an average of 696 J/g SiO_2. These three lime pastes are the control CB9 in elevated pH solution, CB9 with 250mM EDTA in elevated pH solution, and CB30 with 250mM EDTA without pH elevation tested at 30 ℃. These two CB9 mixtures had identical cumulative heat curves and similar reaction kinetics. The concerned CB30 mixture, on the other hand, shows a different cumulative heat curve, which suggests a different reaction kinetics.

The conclusions of this study may also be extended to the development of high-performance cementitious materials in construction and civil infrastructures. However, the exact effect of EDTA on cement hydration and related reaction kinetics needs to be further studied.

References

ACI Committee 236 and 241. (2017). *241R-17: Report on Application of Nanotechnology and Nanomaterials in Concrete*, American Concrete Institute, Farmington Hills, MI, 36.

Aïtcin, P.-C., and Flatt, R. J. (2016). *Science and Technology of Concrete Admixtures*, Elsevier/Woodhead Publishing.

Alvarez, J. I., Fernández, J. M., Navarro-Blasco, I., Duran, A., and Sirera, R. (2013). "Microstructural consequences of nanosilica addition on aerial lime binding materials: Influence of different drying conditions." *Materials Characterization*, 80, 36–49. https://doi.org/10.1016/j.matchar.2013.03.006.

Ayral, A., Julbe, A., Roualdes, S., Rouessac, V., Durand, J., and Sala, B. (2006). "Silica membranes - Basic principles." *Periodica Polytechnica: Chemical Engineering*. 50.

Basma, A.A., and Tuncer, E.R. (1991). "Effect of lime on volume change and compressibility of expansive clays." *Transportation Research Record*, 1295, 52–61.

Belkowitz, J. S., Belkowitz, W. B. , Best, M. A., and Fisher F. T. (2014). "Colloidal silica admixture." *Concrete International*, 36(7).

Bras, A., and Henriques, F. M. A. (2012). "Natural hydraulic lime based grouts – the selection of grout injection parameters for masonry consolidation." *Construction and Building Materials*, 26(1), 135-144. https://doi.org/10.1016/j.conbuildmat.2011.05.012.

Chen, H., Feng, P., Ye, S., and Sun, W. (2018). "The coupling effect of calcium concentration and pH on early hydration of cement." *Construction and Building Materials*, 185, 391–401. https://doi.org/10.1016/j.conbuildmat.2018.07.067.

Davies, M., and Scott, P.J.B. (2006). *Oilfield water technology*, NACE International, Houston, TX.

Diamond, S., and Kinter, E. B. (1965). "Mechanisms of soil-lime stabilization: an interpretive review." *Highway Research Record*, 92, 83–102. http://onlinepubs.trb.org/onlinepubs/hrr/1965/92/92-006.pdf.

Fernández, J. M., Duran, A., Navarro-Blasco, I., Lanas, J., Sirera, R., and Alvarez, J. I. (2013). "Influence of nanosilica and a polycarboxylate ether superplasticizer on the performance of lime mortars." *Cement and Concrete Research*, 43, 12–24. https://doi.org/10.1016/j.cemconres.2012.10.007.

Hosseini, P., Abolhasani, M., Mirzaei, F., Kouhi Anbaran, M. R., Khaksari, Y., and Famili, H. (2018). "Influence of two types of nanosilica hydrosols on short-term properties of sustainable white portland cement mortar." *Journal of Materials in Civil Engineering*, 30(2). https://doi.org/10.1061/(asce)mt.1943-5533.0002152.

Hosseini, P., Booshehrian, A., and Farshchi, S. (2010). "Influence of nano-SiO_2 addition on microstructure and mechanical properties of cement mortars for ferrocement." *Transportation Research Record: Journal of the Transportation Research Board*, 2141(1), 15–20. https://doi.org/10.3141/2141-04.

Iler, R. K. (1979). *The Chemistry of Silica: Solubility, Polymerization, Colloid and Surface Properties and Biochemistry of Silica*, New York, NY: John Wiley and Sons.

Joju, M.R., and Chandrakaran, S. (2021). "Comparative Study on Stabilization of Marine Clay Using Nano-Silica and Lime." *Problematic Soils and Geoenvironmental Concerns, Lecture Notes in Civil Engineering*, 88. Springer, Singapore. https://doi.org/10.1007/978-981-15-6237-2_34.

Kannan, G., and Sujatha, E. R. (2021). "A review on the choice of nano-silica as soil stabilizer." *Silicon*. 14, 6477–6492. https://doi.org/10.1007/s12633-021-01455-z.

Khaloo, A., Mobini, M. H., and Hosseini, P. (2016). "Influence of different types of nano-SiO_2 particles on properties of high-performance concrete." *Construction and Building Materials*, 113, 188–201. https://doi.org/10.1016/j.conbuildmat.2016.03.041.

Kosmatka, S., and Wilson, M. (2011). *Design and Control of Concrete Mixtures*, 15th edition, Portland Cement Association, Skokie, IL, 460.

Kulik, D. A., Wagner, T., Dmytrieva, S. V., Kosakowski, G., Hingerl, F. F., Chudnenko, K. V., and Berner, U. R. (2013). "Gem-selektor geochemical modeling package: Revised algorithm and GEMS3K numerical kernel for coupled simulation codes." *Computational Geosciences*. 17, 1–24. https://doi.org/10.1007/s10596-012-9310-6.

Liao, Y., Gui, Y., Wang, K., Al Qunaynah, S., Bawa, S. M., and Tang, S. (2021). "Activation energy of calcium sulfoaluminate cement-based materials." *Materials and Structures*, 54, 162. https://doi.org/10.1617/s11527-021-01753-3.

Lothenbach, B., Kulik, D. A., Matschei, T., Balonis, M., Baquerizo, L., Dilnesa, B., Miron, G. D., and Myers, R. J. (2019). "Cemdata18: A chemical thermodynamic database for hydrated Portland cements and alkali-activated materials." *Cement and Concrete Research*, 115, 472–506. https://doi.org/10.1016/j.cemconres.2018.04.018.

Luo, K., Li, J., Lu, Z., Jiang, J., and Niu, Y. (2019). "Effect of nano-SiO_2 on early hydration of natural hydraulic lime." *Construction and Building Materials*, 216, 119–127. https://doi.org/10.1016/j.conbuildmat.2019.04.269.

Madani, H., Bagheri, A., and Parhizkar, T. (2012). "The pozzolanic reactivity of monodispersed nanosilica Hydrosols and their influence on the hydration characteristics of Portland cement." *Cement and Concrete Research*, 42(12), 1563–1570. https://doi.org/10.1016/j.cemconres.2012.09.004.

Maddalena, R., Hall, C., and Hamilton, A. (2019). "Effect of silica particle size on the formation of calcium silicate hydrate [C-S-H] using thermal analysis." *Thermochimica Acta*, 672, 142–149. https://doi.org/10.1016/j.tca.2018.09.003.

Metaxa, Z. S., Tolkou, A. K., Efstathiou, S., Rahdar, A., Favvas, E. P., Mitropoulos, A. C., and Kyzas, G. Z. (2021). "Nanomaterials in cementitious composites: An update." *Molecules*, 26(5), 1430. https://doi.org/10.3390/molecules26051430.

Moon, J., Taha, M., Youm, K.-S., and Kim, J. (2016). “Investigation of pozzolanic reaction in nanosilica-cement blended pastes based on solid-state kinetic models and ^{29}SI MAS NMR.” *Materials*, 9(2), 99. https://doi.org/10.3390/ma9020099.

Moropoulou, A., Cakmak, A., Labropoulos, K. C., Van Grieken, R., and Torfs, K. (2004). “Accelerated microstructural evolution of a calcium-silicate-hydrate (C-S-H) phase in pozzolanic pastes using fine siliceous sources: Comparison with historic Pozzolanic mortars.” *Cement and Concrete Research*, 34(1), 1–6. https://doi.org/10.1016/s0008-8846(03)00187-x.

Mouillet, V., Séjourné, D., Delmotte, V., Ritter, H.-J., and Lesueur, D. (2014). “Method of quantification of hydrated lime in asphalt mixtures.” *Construction and Building Materials*, 68, 348–354. https://doi.org/10.1016/j.conbuildmat.2014.06.063.

Nunes, C., Slížková, Z., Stefanidou, M., and Němeček, J. (2016). “Microstructure of lime and lime-pozzolana pastes with nanosilica.” *Cement and Concrete Research*, 83, 152–163. https://doi.org/10.1016/j.cemconres.2016.02.004.

Phanikumar, B. R. (2009). “Effect of lime and fly ash on swell, consolidation and shear strength characteristics of expansive clays: a comparative study.” *Geomechanics and Geoengineering: An International Journal*, 4:2, 175-181. https://doi.org/10.1080/17486020902856983.

Pu, S. Y., Zhu, Z. D., Wang, H. R., Song, W. L., and Wei, R. J. (2019). “Mechanical characteristics and water stability of silt solidified by incorporating lime, lime and cement mixture, and SEU-2 binder.” *Construction and Building Materials*, 214, 111–120. https://doi.org/10.1016/j.conbuildmat.2019.04.103.

Qing, Y., Zenan, Z., Li, S., and Rongshen, C. (2006). “A comparative study on the pozzolanic activity between nano-SiO_2 and silica fume.” *Journal of Wuhan University of Technology-Mater. Sci.* 21(3), 153–157. https://doi.org/10.1007/bf02840907.

Reches, Y., Thomson, K., Helbing, M., Kosson, D. S., and Sanchez, F. (2018). “Agglomeration and reactivity of nanoparticles of SiO_2, TiO_2, Al_2O_3, Fe_2O_3, and clays in cement pastes and

effects on compressive strength at ambient and elevated temperatures." *Construction and Building Materials*, 167, 860–873. https://doi.org/10.1016/j.conbuildmat.2018.02.032.

Santoro, L., Volpicelli, G., and Caprio, V. (1987). "Limestone neutralization of acid waters in the presence of surface precipitates." *Water Research*, 21(6), 641–647. https://doi.org/10.1016/0043-1354(87)90074-1.

Sargam, Y., and Wang, K. (2021). "Hydration kinetics and activation energy of cement pastes containing various nanoparticles." *Composites Part B: Engineering*, 216, 108836. https://doi.org/10.1016/j.compositesb.2021.108836.

Snellings, R., Mertens, G., and Elsen, J. (2012). "Supplementary cementitious materials." *Reviews in Mineralogy and Geochemistry*, 74(1), 211–278. https://doi.org/10.2138/rmg.2012.74.6.

Stefanidou, M., and Papayianni, I. (2005). "The role of aggregates on the structure and properties of lime mortars." *Cement and Concrete Composites*, 27(9-10), 914–919. https://doi.org/10.1016/j.cemconcomp.2005.05.001.

Thomas, N. L., and Double, D. D. (1983). "The hydration of Portland cement, C_3S and C_2S in the presence of a calcium complexing admixture (EDTA)." *Cement and Concrete Research*, 13(3), 391–400. https://doi.org/10.1016/0008-8846(83)90039-x.

Vyazovkin, S., and Wight, C. A. (1997). "Kinetics in solids." *Annual Review of Physical Chemistry*, 48, 125–149. https://doi.org/10.1146/annurev.physchem.48.1.125.

Wagner, T., Kulik, D. A., Hingerl, F. F., and Dmytrieva, S. V. (2012). "Gem-Selektor Geochemical Modeling Package: TSolMod Library and data interface for multicomponent phase models." *The Canadian Mineralogist*, 50(5), 1173–1195. https://doi.org/10.3749/canmin.50.5.1173.

Yajun, J., and Cahyadi, J. H. (2004). "Simulation of silica fume blended cement hydration." *Materials and Structures*, 37(270), 397–404. https://doi.org/10.1617/12684.

Zhang, H., Ma, S., and Wu, Y. (2011). *Building Materials in Civil Engineering*. Oxford: Woodhead Pub.

Zhuang, C., and Chen, Y. (2019). “The effect of nano-SiO_2 on concrete properties: A review.” *Nanotechnology Reviews*, 8, 562–572. https://doi.org/10.1515/ntrev-2019-0050.

Appendix A

Fig. A.1 shows the particle size distribution of calcium hydroxide and silica nanoparticles. Figs A.2 and A.3 present the results of TGA on lime paste containing 250mM oxalic acid at 28 days of reaction and pure calcium oxalate as a reference material, respectively. As can be seen in Fig. A.3, calcium oxalate has three distinct decomposition stages which can be found in TGA results for the lime paste containing oxalic acid. As seen in Figs A.2 and A.3, the second peak in derivate thermogravimetric curve (DTG) can be related to the decomposition of both calcium hydroxide and calcium oxalate making it difficult to interpret the TGA results and calculate the consumed quantity of calcium hydroxide.

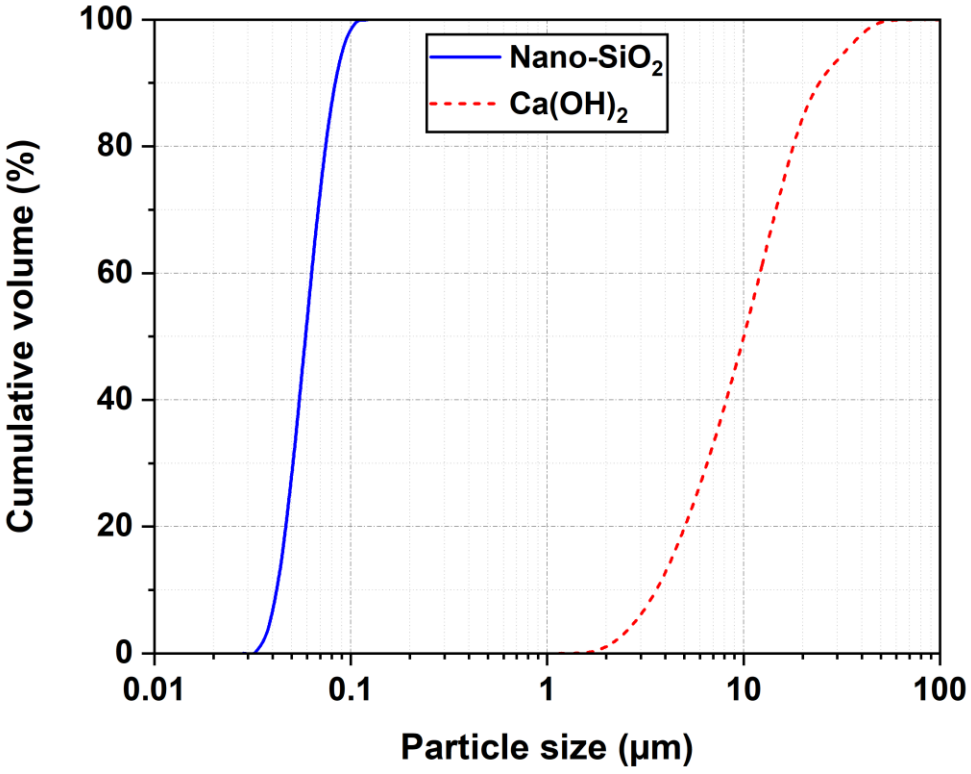

Fig. A.1 Particle size distribution of calcium hydroxide and silica nanoparticles.

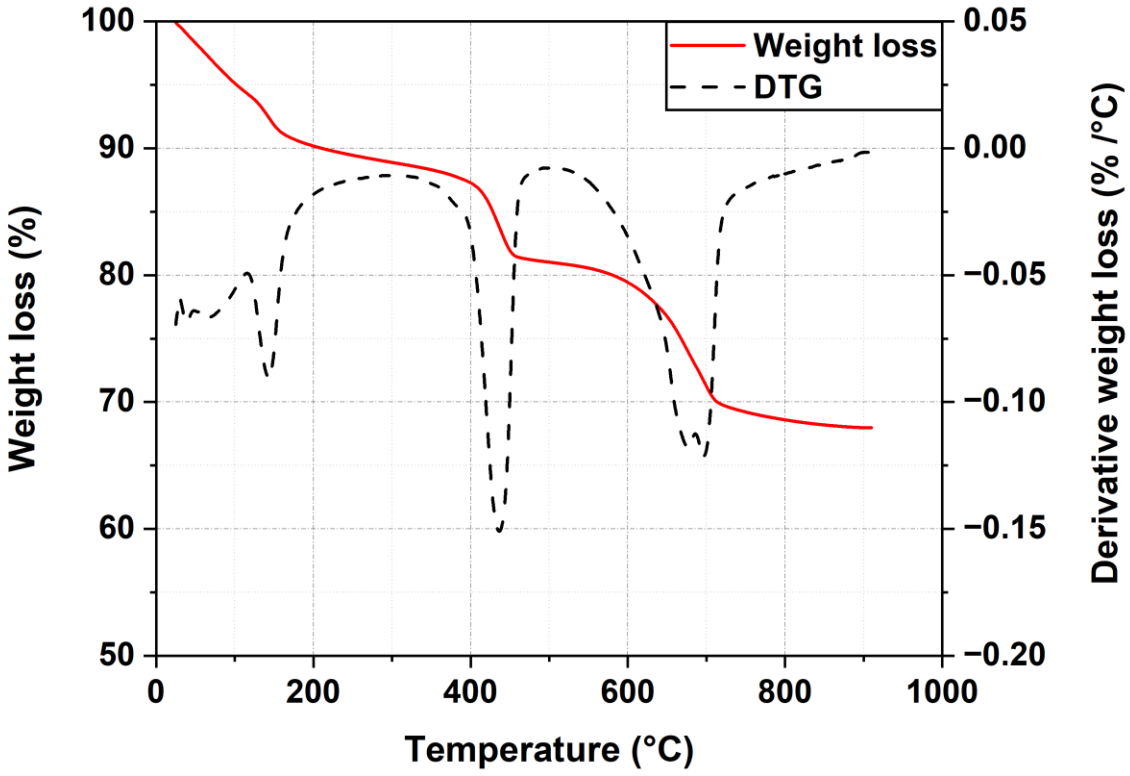

Fig. A.2 TGA of lime paste with 250mM oxalic acid at the age of 28 days.

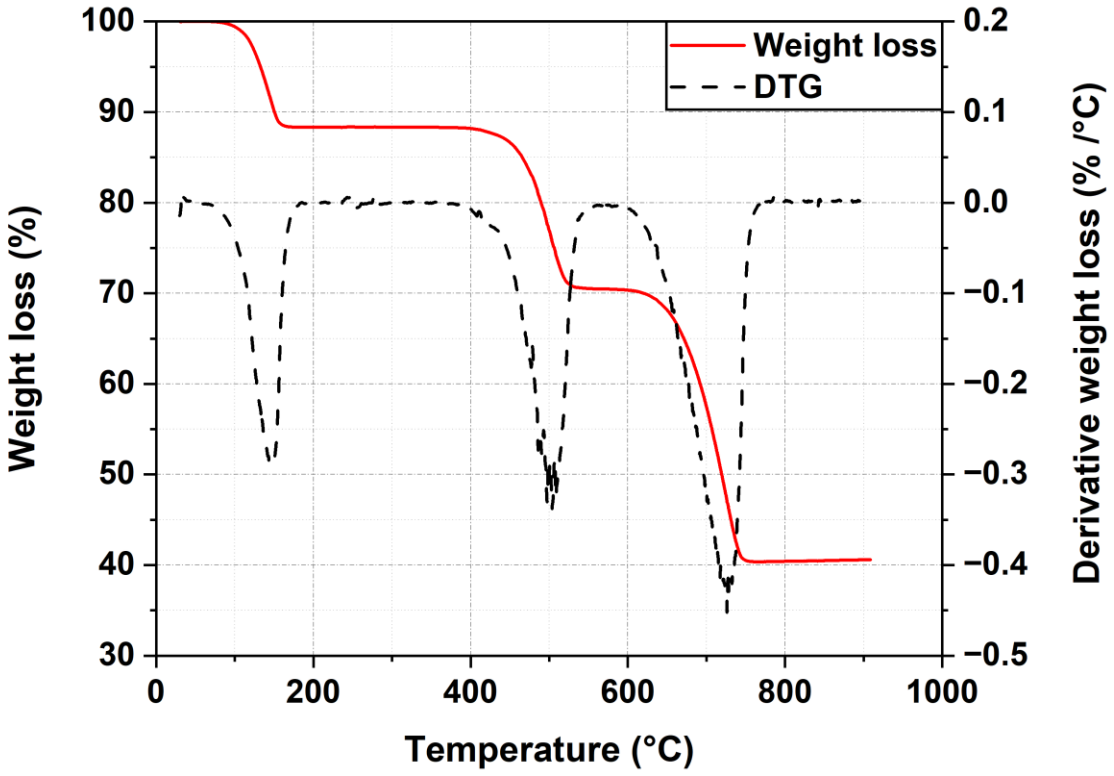

Fig. A.3 TGA of pure calcium oxalate sample.

Appendix B

Figures B.1 to B.8 show the fitting equations used in the exponential technique to calculate apparent activation energy.

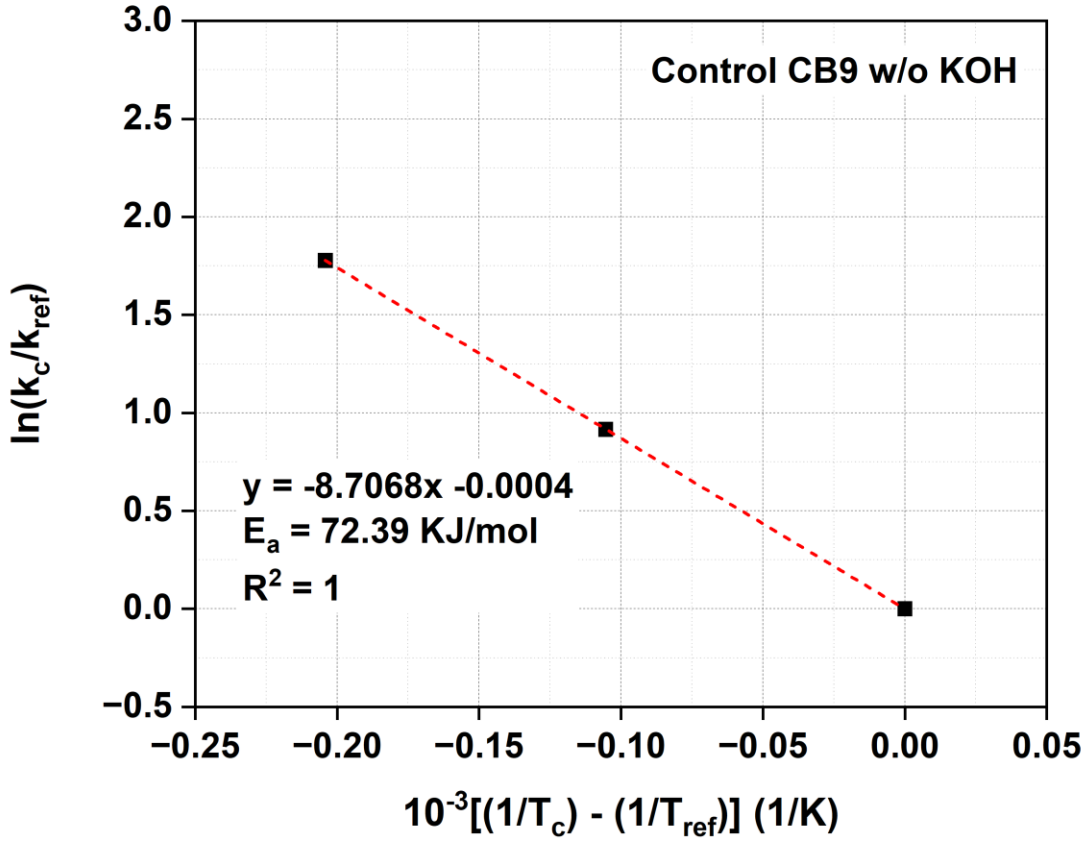

Figure B.1 The fitting equation used in the exponential technique to calculate the apparent activation energy of the control lime mixture containing CB9 without KOH.

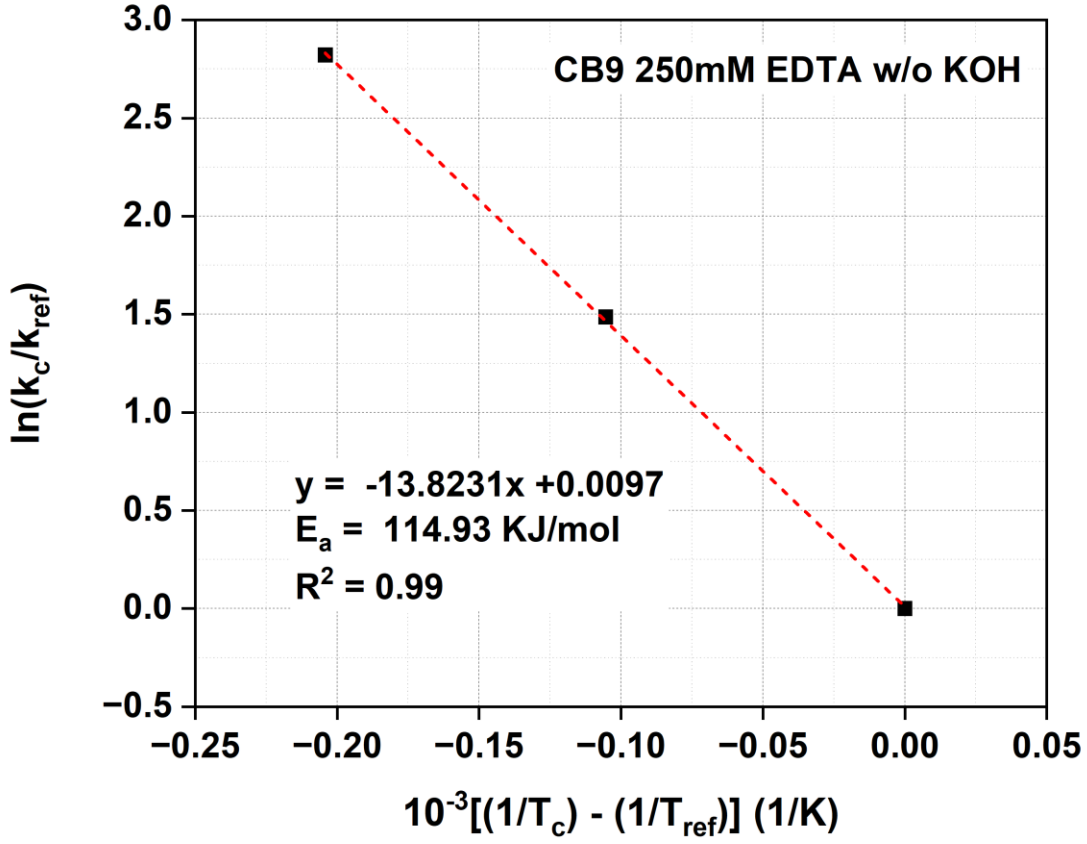

Figure B.2 The fitting equation used in the exponential technique to calculate the apparent activation energy of the lime mixture containing CB9 with 250mM EDTA and without KOH.

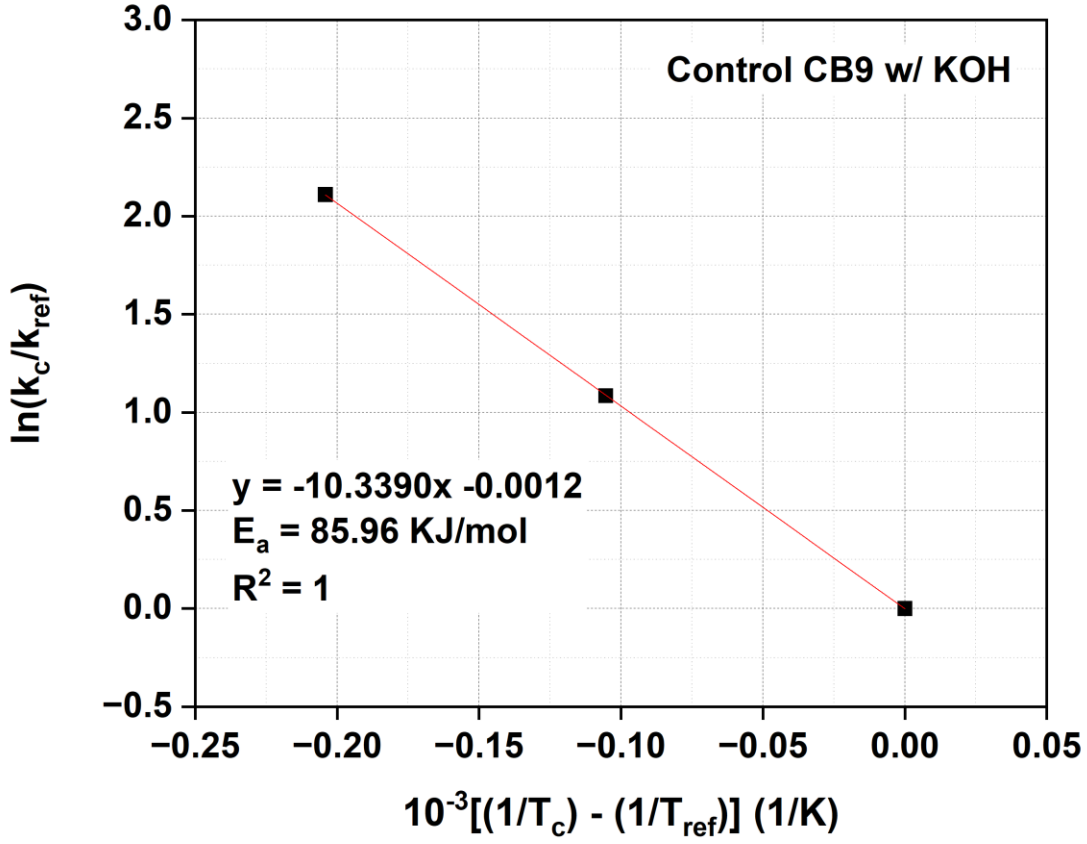

Figure B.3 The fitting equation used in the exponential technique to calculate the apparent activation energy of the lime mixture containing CB9 with KOH.

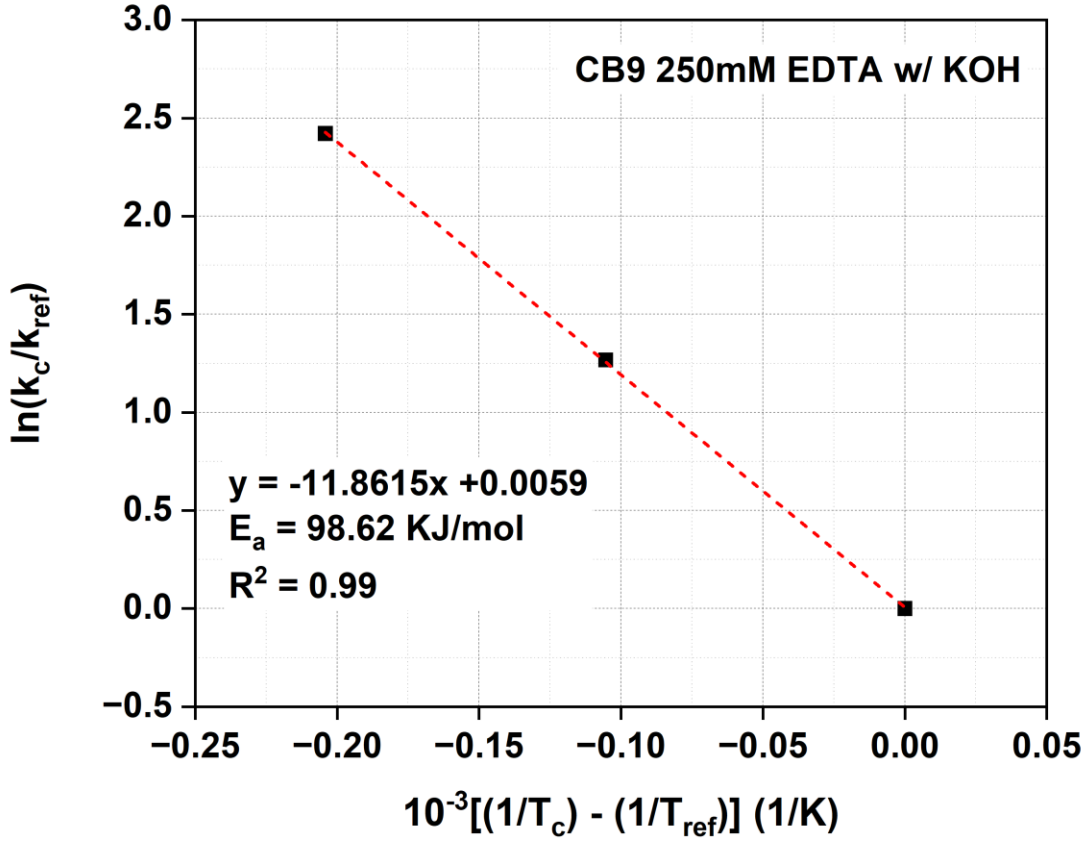

Figure B.4 The fitting equation used in the exponential technique to calculate the apparent activation energy of the lime mixture containing CB9 with 250mM EDTA and KOH.

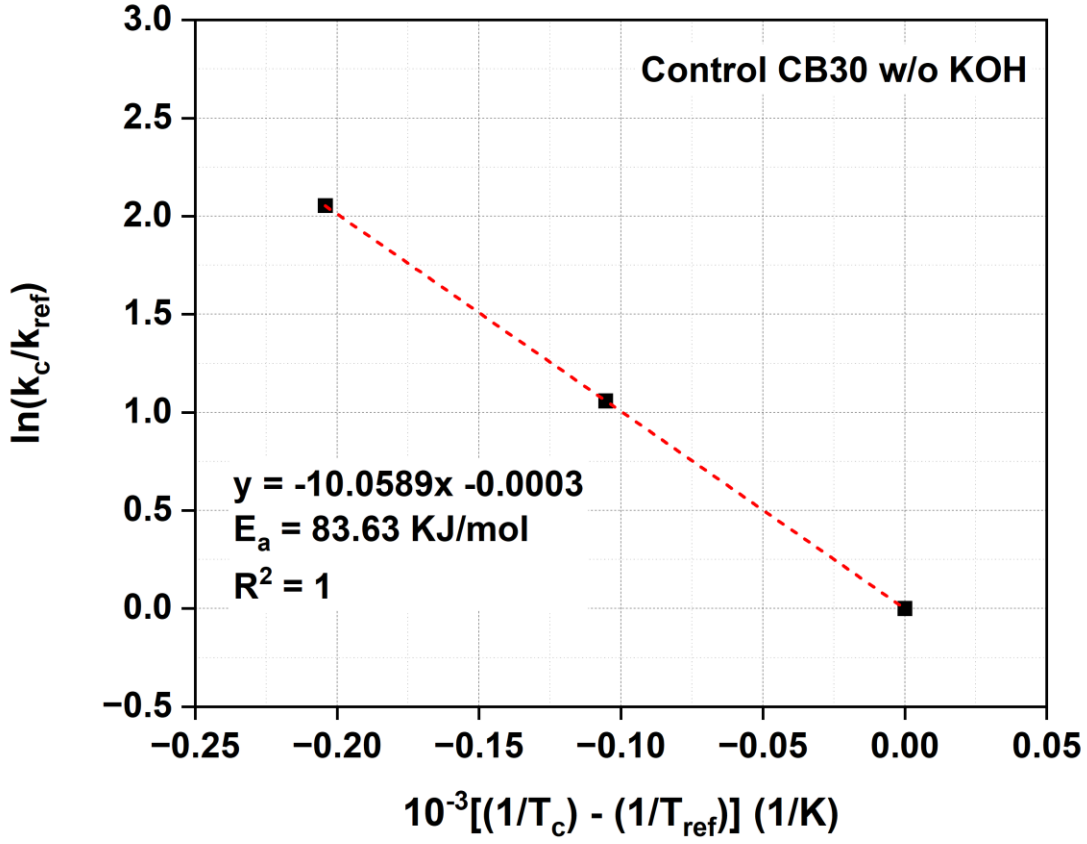

Figure B.5 The fitting equation used in the exponential technique to calculate the apparent activation energy of the control lime mixture containing CB30 without KOH.

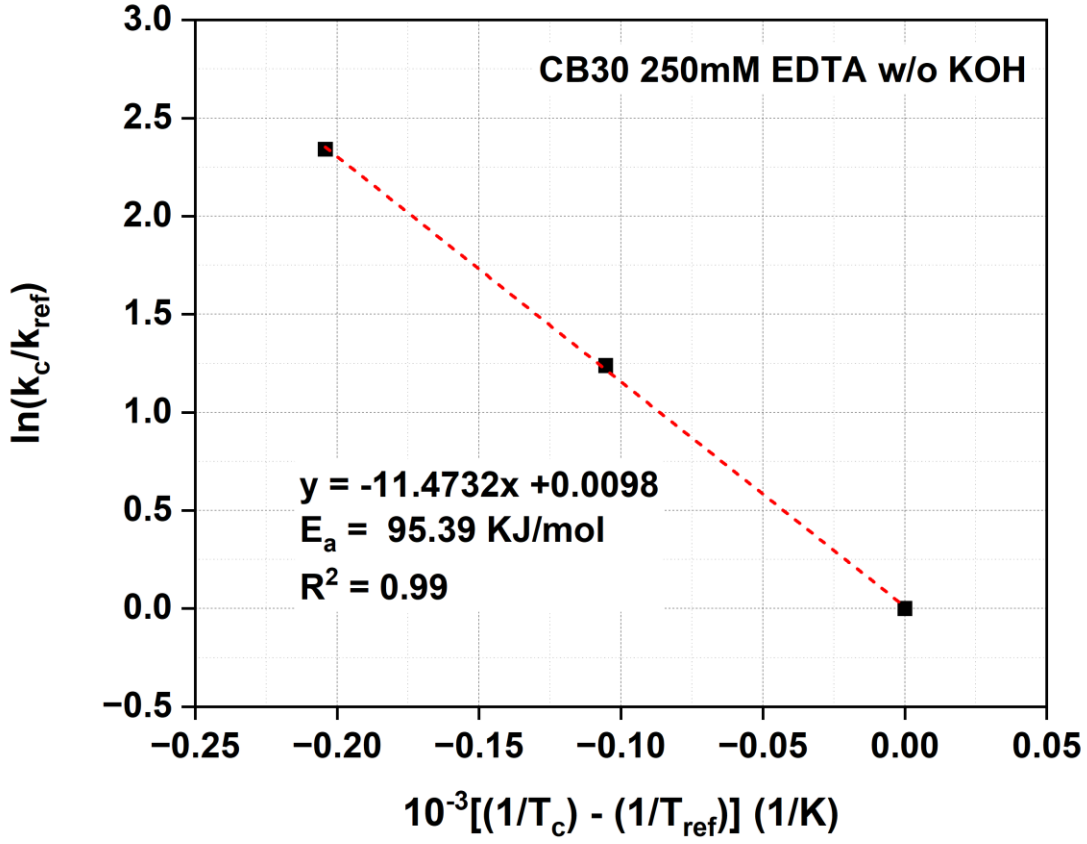

Figure B.6 The fitting equation used in the exponential technique to calculate the apparent activation energy of the lime mixture containing CB30 with 250mM EDTA and without KOH.

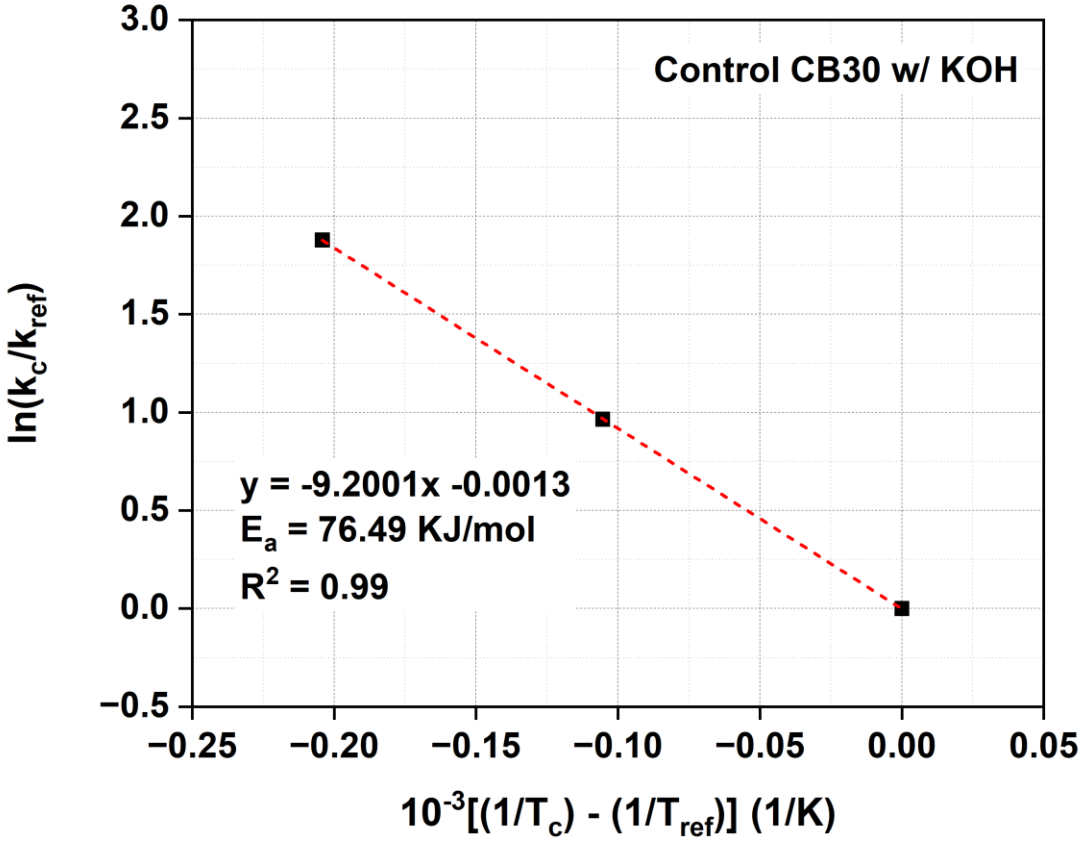

Figure B.7 The fitting equation used in the exponential technique to calculate the apparent activation energy of the lime mixture containing CB30 with KOH.

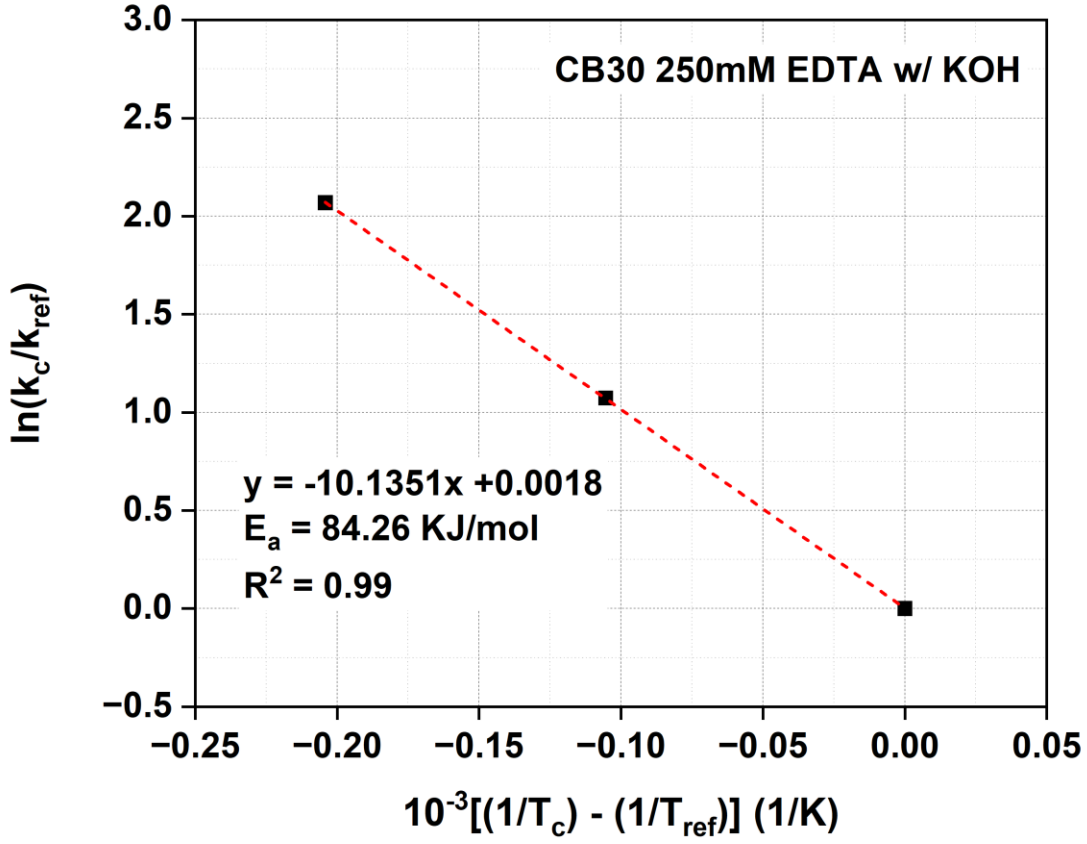

Figure B.8 The fitting equation used in the exponential technique to calculate the apparent activation energy of the lime mixture containing CB30 with 250mM EDTA and KOH.

Vitae

Abbas completed his bachelor's and master's studies in civil engineering at King Fahd University of Petroleum and Minerals (KFUPM), Dhahran, Saudi Arabia, in 2013 and 2016, respectively. He was a graduate assistant for five years (2013 to 2018) and then a lecturer in the civil and environmental engineering department at KFUPM. Throughout his profession at KFUPM, he was involved in educational works and assisted in cooperative and summer internship programs for undergraduate students. Also, he was a member of the public relations committee at the civil and environmental engineering department. His master's thesis was an experimental study on the development of geopolymer concrete incorporating local waste materials. He was then awarded a scholarship to study for his Ph.D. in the United States. In his Ph.D. at the University of Wisconsin - Madison, Abbas and his thesis advisor Prof. Bu Wang are investigating the possibility of dispersing silica nanoparticles in cementitious media. In spring 2022, Abbas is becoming a faculty member in the civil and environmental engineering department at KFUPM.